Mitigating Spatial-Wideband and Beam-Split Effects via Distributed IRSs: Design and Analysis

L. Yashvanth, *Student Member, IEEE*, Chandra R. Murthy, *Fellow, IEEE*, and Bhaskar D. Rao, *Life Fellow, IEEE*

***Abstract*—This paper addresses the mitigation of spatial-wideband (SW) and the resulting beam-split (B-SP) effects in intelligent reflecting surface (IRS)-aided wideband systems. The SW effect occurs when the signal delay across the IRS aperture exceeds the system's sampling duration, causing the user equipment's (UE) channel angle to vary with frequency. This leads to the B-SP effect, wherein the IRS cannot coherently beamform to a given UE over the entire bandwidth, reducing array gain and throughput. We first show that partitioning a single IRS into multiple smaller IRSs and distributing them in the environment can naturally mitigate the SW effect (and hence the B-SP effect) by parallelizing the spatial delays and exploiting angle diversity benefits. Next, by determining the maximum number of elements at each smaller IRS to limit B-SP effects and analyzing the achievable sum-rate, we demonstrate that our approach ensures a minimum positive rate over the entire bandwidth of operation. However, distributed IRSs may introduce temporal delay spread (TDS) due to the differences in the path lengths through the IRSs and this may reduce the achievable flat channel gain. To minimize TDS and maintain the full array gain, we show that the optimal placement of the IRSs is on an ellipse with the base station (BS) and UE as the focal points. We also analyze the impact of the optimal IRS placement on TDS and throughput for a UE that is located within a hotspot served by the IRSs. Finally, we illustrate that distributed IRSs enhance angle diversity, which exponentially reduces the outage probability due to B-SP effects as the number of IRSs increases. Numerical results validate the efficacy and simplicity of our method compared to the existing solutions.**

***Index Terms*—Distributed IRS, spatial-wideband effect, beam-squint and beam-split effects, OFDM, angle diversity.**

I. Introduction

Intelligent reflecting surfaces (IRS) are envisioned to improve the performance of wireless systems by beamforming signals in desired directions using independently reconfigurable passive phase shifters [2]–[4]. One of the key use cases for IRSs is to create a *virtual line-of-sight (LoS) path* to multiple user equipments (UEs) clustered in a hotspot area when the LoS path between the hotspot and a base station (BS) is obstructed. However, the cascaded link via the IRS encounters a multiplicative path loss, and an IRS with a large number of elements has to be used to achieve appreciable benefits [5]. Large arrays cause the signal delay across the aperture to be comparable to or even exceed the sampling duration. This results in *spatial-wideband* (SW) effects [6], which manifests as the beam-squint (B-SQ) and *beam-split* (B-SP) effects in the frequency domain, and severely degrades the array gain and throughput at a UE. This paper addresses this problem by using distributed IRSs which naturally mitigate the SW and B-SP effects at almost no additional complexity.

L. Yashvanth and Chandra R. Murthy are with the Department of Electrical Communication Engineering, Indian Institute of Science, Bengaluru, India 560 012. (e-mails: {yashvanthl, cmurthy}@iisc.ac.in.) Bhaskar D. Rao is with the Department of Electrical and Computer Engineering, University of California, San Diego, CA 92092 USA (e-mail: brao@ucsd.edu).

The work of L. Yashvanth was financially supported by the Prime Minister's Research Fellowship, that of Chandra R. Murthy was supported by the Qualcomm 6G UR India Grant, and that of Bhaskar D. Rao was supported by the National Science Foundation (NSF) Grant CCF-2225617.

A part of this work was presented at the IEEE International Conference on Acoustics, Speech and Signal Processing (ICASSP), 2025 [1].

A. Beam-Split: The Curse of the Spatial-Wideband Effect

In high-frequency millimeter wave (mmWave) bands, where large bandwidths (BW) are used, the channel between two nodes is typically directional because there are only a few significant scatterers. These directions are independent of the operating frequencies as long as the delay spread of the channel is much smaller than the system sampling duration, known as the *narrowband* condition. However, when an IRS with a large number of elements is used, the spatial delay spread across the aperture can easily exceed the sampling period and violate the narrowband condition. This results in the spatial-wideband effect, where even an LoS channel becomes frequency-selective.

In this scenario, the main challenge is that the IRS fails to coherently beamform across the entire BW allotted to a UE in the system. Specifically, when the IRS is configured as a phased array tuned to a specific frequency component within the BW, e.g., the carrier frequency (which is typically the case), the SW effect induces the B-SQ and B-SP effects in the frequency domain, which severely degrades the array gain at other frequencies within the BW. In the B-SQ effect, the beam formed by the IRS squints at different angles across frequencies, though the angular spread across the BW remains within the main lobe of the beam. In contrast, the B-SP is a more severe form of B-SQ and occurs when the number of IRS elements or allotted BW (or both) further increases. In the B-SP effect, the beam formed by the IRS at the tuned frequency splits into distinct, resolvable beams on other frequencies within the BW. Consequently, the IRS fails to beamform and constructively combine signals at the UE over the full BW, severely degrading the achievable channel gain and spectral efficiency. While the SW effects can be circumvented by reducing the number of IRS elements or the total BW, this also lowers the achievable channel gain and system throughput. Therefore, it is crucial to design efficient methods, preferably with low complexity, to mitigate SW and the resulting B-SP effects in IRS-aided wideband systems.

B. Related Work & Motivation

Most existing studies on IRS-aided systems overlook the B-SP effects resulting from the SW effects and end up overestimating the achievable benefits of an IRS. Only a few works address the wideband effects; we summarize them below.

In [7], [8], and [9], methods for channel estimation and beam training were developed accounting for the SW effects. Localization of UEs using SW effects was discussed in [10]. Optimization of IRS phases to maximize the sum-rate in orthogonal frequency division multiplexing (OFDM) systems with B-SQ effects was studied in [11]. In [12] and [13], joint optimization of the IRS configuration and BS precoder was explored for multiple-input multiple-output (MIMO) terahertz systems. In [14], the achievable ergodic rate of a MIMO-OFDM system with B-SQ effects was examined, and [15] solved for optimal IRS configuration to maximize the signal-to-interference-plus-noise ratio (SINR) with B-SQ effects. Finally, [16] analyzes the coverage in the presence of B-SQ effects, and [17] optimizes IRS configurations to control the width of the beams in an OFDM-based multiple access system.

Along the lines of mitigating the SW (and hence the B-SP effects), existing works often use true time-delay (TTD) units at the IRS to compensate for the excess signal delay across the aperture, thereby eliminating the SW effects [18]. In [19], a hardware-efficient design of TTD-enabled IRS was investigated, and [20] used delay-phase units to eliminate the B-SP effects in both far-field and near-field scenarios. In [21], the TTDs and BS precoder were jointly optimized to maximize the sum-rate of a multi-user system, and [22] used TTDs to design an efficient IRS-aided cell-free wideband MIMO system. Further, in [23], TTD units were proposed as a means to mitigate B-SP effects in holographic RIS-assisted systems. In contrast, [24] utilized TTD units to control the B-SP effect for improving the accuracy of sensing multiple UEs in the network. However, using TTD units at an IRS presents a number of challenges: 1) the number of TTD units increases with the number of IRS elements, requiring more hardware and space; 2) high-resolution TTDs are necessary for precise delay compensation, which increases power consumption, and 3) since the IRS elements continuously receive signals from the BS, apply a delay, and then reflect the signal toward the UE, the overall operation becomes full-duplex in nature. This introduces self-interference (SI) at each IRS element, and to alleviate it, sophisticated SI cancellation techniques are required at each element of the IRS [25], which further complicates the design and hardware requirements. These issues can potentially undermine the hardware cost and energy efficiency benefits of using IRSs. In particular, to the best of our knowledge, no paper in the literature describes the hardware implementation and demonstration of a TTD-enabled IRS. Yet another approach is to virtually partition a single large IRS into multiple sub-IRSs, with each sub-IRS optimized to the channels over distinct frequency bands [26]. Although this provides a flat response across the BW, the achievable array gain scales only with the number of elements at a sub-IRS and not with the total number of IRS elements. Finally, while [27], [28] suggest that multiple IRSs can reduce the impact of B-SQ, they do not analyze the performance of distributed IRSs accounting for B-SQ or explicitly design a distributed IRS architecture to mitigate these wideband effects.

To address the above issues, in this paper, we propose an alternative approach without relying on TTDs and use a distributed IRS design instead of a single large IRS. We show that, when properly designed, a distributed IRS can inherently overcome the SW effect without increasing complexity or sacrificing performance.[1]

C. Contributions & Takeaways

We now list the key contributions of our paper.

1) **SW effect reduction:** We mathematically show that a distributed IRS design naturally parallelizes the spatial delays and mitigates the SW effect. (See Sec. III-A.)
2) **Number of IRS elements**: We determine the maximum number of elements at each IRS so that the loss in the array gain due to B-SP is within acceptable limits while retaining the achievable peak gain. (See Theorem 1.)
3) **Sum-rate and array gain:** Next, we analyze the impact of the *temporal delay spread* (TDS) caused by multiple paths arriving at the UE through different IRSs. We show that the achievable rate on every subcarrier (SC) scales log-quadratically in the number of elements at each IRS and at least log-linearly in the number of IRSs, thus effectively mitigating deep nulls in the channel response due to the B-SP effect. Further, when the TDS is zero, the sum-rate across all the SCs spanning the BW grows log quadratically in the total number of IRS elements. (See Theorem 2.)
4) **Optimizing the IRS locations:** Having noted that the value of TDS is crucial in determining the achievable flat channel gain, we next focus on optimizing the IRS locations:
   a) *Single UE:* To minimize the TDS at a single UE, we show that it is optimal to position the IRSs on an ellipse with the locations of BS and UE as its foci. The optimal TDS then becomes zero. (See Theorem 3.)
   b) *Multiple UEs:* With multiple UEs located within a hotspot, we position the IRSs over an ellipse whose foci are given by the location of the BS and centroid of the distribution of the UE locations. We derive the achievable TDS at an arbitrary location and subsequently characterize a lower bound on the achievable sum-rate using the distributed IRSs. (See Prop. 1 and Theorem 4.)
5) **Angle diversity gain:** Finally, we reveal that multiple IRSs additionally introduce angle diversity gain due to multiple independent paths seen by the UE. In particular, we show that the probability that the array gain equals the worst-case acceptable value (due to the residual B-SQ) decreases exponentially with the number of IRSs. On the other hand, the outage probability of a centralized IRS for a target SNR close to the peak array gain is bounded away from zero as the number of IRS elements increases. (See Theorem 5.)

We numerically validate our results and illustrate the efficacy of our solution in mitigating the SW and the resulting B-SP effects. For instance, when the BW is 400 MHz around $f_c = 30$ GHz, with a total of 1024 IRS elements, if we use a centralized large IRS, only 12.5% of the total BW gets an array gain which is within 3 dB of the peak array gain. On the other hand, if we deploy 8 distributed IRSs, each with 128 elements,

[1]Note that B-SQ and B-SP effects can arise in both far-field and near-field scenarios [20]. To illustrate our core idea, this paper will focus on the case where the BS/UEs are in the far-field of IRS(s). Extensions to near-field scenarios will be considered for future work.

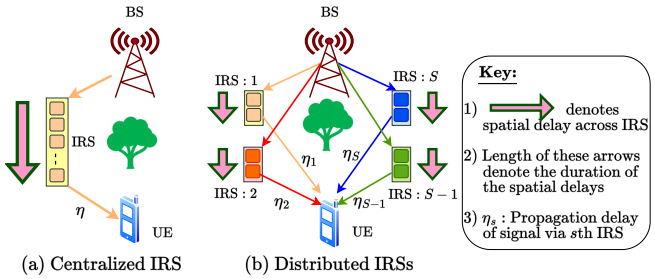

(a) Centralized IRS (b) Distributed IRSs

Fig. 1: Distributed IRSs reduce spatial delays and mitigate SW & B-SP effects. The TDS is 0 only when the propagation delays are equal: $\eta_1 = \eta_2 \ldots = \eta_S$.

the entire 400 MHz BW obtains an array gain that is within the 3 dB margin of the peak array gain (see Fig. 6). As a result, the difference in the sum-rate obtained with the distributed IRS and the TTD-enabled IRS (which completely eliminates the B-SP, albeit at a higher complexity) is less than 0.5 bps/Hz (see Fig. 7.) Finally, even with finite TDS, distributed IRS still procures a far superior performance over the centralized case, with the sum-rate exhibiting log-quadratic growth in the total number of IRS elements. (see Fig. 10.) Thus, distributed IRS mitigates B-SP effects and provides the full array gain over the entire BW at almost no added complexity.

Notation: $\lfloor\cdot\rfloor, \lceil\cdot\rceil$ denote the floor and ceil functions; $\mathcal{U}[a,b]$ denotes a uniform distribution with support $[a,b]$; $\mathsf{Pr}(\cdot)$ and $\mathbb{E}[\cdot]$ stand for the probability measure and expectation operator; $\|\cdot\|_p$ refers to the ℓ_p vector norm; $\mathcal{O}(\cdot)$ is the Landau's Big-O function; $\mathbb{R}, \mathbb{C}$ stand for real and complex numbers.

II. System Model

A. Channel Impulse Response and Spatial-Wideband Effect

Consider the system depicted in Fig. 1(a), where a BS communicates with a UE, and is assisted by an N-element IRS in the mmWave frequency band. For simplicity, and following past work in the area, we assume that the IRS is implemented as a uniform linear array (ULA) with inter-element spacing denoted by d [7], [11], [20], [21]. The baseband impulse response of the channel from the BS to the nth IRS element is given by [19][2]

$$h_{1,n}(t) = \sqrt{\alpha}\delta\left(t - \eta^{(1)} - (n-1)\frac{d}{c}\sin(\psi)\right) \times e^{-j2\pi f_c \eta^{(1)}} \times e^{-j2\pi f_c (n-1)\frac{d}{c}\sin(\psi)}, \quad (1)$$

where α, $\eta^{(1)}$, f_c, and ψ represent the path-loss, propagation delay in the link from BS to a reference element (either the first or last element, depending on whether ψ is positive or negative) of IRS, the carrier frequency, and the direction of arrival (DoA) of the signal from the BS to the IRS, respectively. Finally, $c = 3 \times 10^8$ m/s denotes the speed of light, and $\delta(t)$ stands for the Dirac-delta function.

Similarly, the baseband impulse response of the channel from the nth IRS element to the UE is

$$h_{2,n}(t) = \sqrt{\gamma}\delta\left(t - \eta^{(2)} + (n-1)\frac{d}{c}\sin(\omega)\right) \times e^{-j2\pi f_c \eta^{(2)}} \times e^{j2\pi f_c (n-1)\frac{d}{c}\sin(\omega)}, \quad (2)$$

[2]We consider a single-antenna BS to specifically analyze the impact of the IRS on system performance. In Sec. III-D, we explain how our results can be extended to scenarios with multiple antennas at the BS.

where γ, $\eta^{(2)}$, and ω denote the path-loss, delay, and direction of departure (DoD) from the IRS to the UE, respectively. Hence, the effective channel from the BS to the UE is[3]

$$\begin{aligned} h(t) &= \sum_{n=1}^{N} \theta_n h_{2,n}(t) \circledast h_{1,n}(t) \\ &= \sum_{n=1}^{N} \theta_n \tilde{h}_1 \tilde{h}_2 \delta\left(t - \eta - (n-1)\frac{d}{c}\left(\sin(\psi) - \sin(\omega)\right)\right) \\ &\qquad \times e^{-j2\pi f_c (n-1)\frac{d}{c}\sin(\phi)}, \end{aligned} \quad (3)$$

where $\tilde{h}_1 \triangleq \sqrt{\alpha}e^{-j2\pi f_c \eta^{(1)}}$, $\tilde{h}_2 \triangleq \sqrt{\gamma}e^{-j2\pi f_c \eta^{(2)}}$, and $\circledast$ stands for the linear convolution operator. Further, θ_n, $\eta \triangleq \eta^{(1)} + \eta^{(2)}$, and $\phi \triangleq \sin^{-1}_{(p)}(\sin(\psi) - \sin(\omega))$ denote the phase shift introduced by the nth IRS element, the total propagation delay, and the effective cascaded angle at the UE, respectively. Also, $\sin^{-1}_{(p)}(x)$ is defined so that $x \in [-1, 1)$, the principal argument of the inverse sine function [29], [30, Eq. 32]. Thus, the *spatial delay spread* of the channel through the IRS is

$$\Delta\tau^{\mathrm{C}} = (N-1)\frac{d}{c}\left|\left(\sin(\psi) - \sin(\omega)\right)\right|. \quad (4)$$

When both N and the BW (denoted by W) are large, the *narrowband* condition: $\Delta\tau^{\mathrm{C}} \ll 1/W$, ceases to hold. Then, the spatial delay incurred by the signal while traversing across the IRS aperture becomes comparable to or more than the sampling duration, leading to the spatial-wideband effect [6]. Then, from (3), the frequency response of the channel is

$$\begin{aligned} H(f) &\overset{(a)}{=} \tilde{h}\sum_{n=1}^{N}\theta_n e^{-j2\pi(n-1)\frac{d}{c}\{f(\sin(\psi)-\sin(\omega))+f_c\sin(\phi)\}} \\ &\overset{(b)}{=} \tilde{h}\sum_{n=1}^{N}\theta_n e^{-j\pi(n-1)\sin(\phi)\left\{1+\frac{f}{f_c}\right\}} \\ &\overset{(c)}{=} \sqrt{N}\tilde{h}\boldsymbol{\theta}^H \mathbf{a}_N\left(\sin^{-1}_{(p)}\left\{(1+(f/f_c))\sin(\phi)\right\}\right), \end{aligned} \quad (5)$$

where, in (a), we absorbed η into receiver timing offset and defined the cascaded channel coefficient as $\tilde{h} \triangleq \tilde{h}_1\tilde{h}_2$; in (b), we set $d = \lambda_c/2$, where λ_c is the carrier wavelength and used the definition of ϕ; in (c), we defined the IRS configuration vector $\boldsymbol{\theta} \triangleq [\theta_1^*, \ldots, \theta_N^*]^T$, where $(\cdot)^*$ stands for complex conjugation and $\mathbf{a}_N(\cdot)$ is the array steering vector given by

$$\mathbf{a}_N(x) \triangleq 1/\sqrt{N}\left[1, e^{-j\pi\sin(x)}, \ldots, e^{-j\pi(N-1)\sin(x)}\right]^T.$$

Therefore, considering an OFDM system with K SCs, the channel on the kth SC is

$$H[k] \triangleq H(f_k) = \sqrt{N}\tilde{h}\boldsymbol{\theta}^H \mathbf{a}_N\left(\sin^{-1}_{(p)}\left\{(1+(f_k/f_c))\sin(\phi)\right\}\right), \quad (6)$$

where f_k is the baseband frequency of the kth SC, given by

$$f_k = -\frac{W}{2} + \frac{W}{2K} + (k-1)\frac{W}{K}, \quad k = 1, \ldots, K.$$

B. The Beam-split Effect

Consider the setting where a BS provides service to a UE over a wide bandwidth, W. Then, in the presence of a large

[3]The direct path from the BS to UE can be blocked/weak compared to the channel via the IRS, so we do not account for direct path in our model [7].

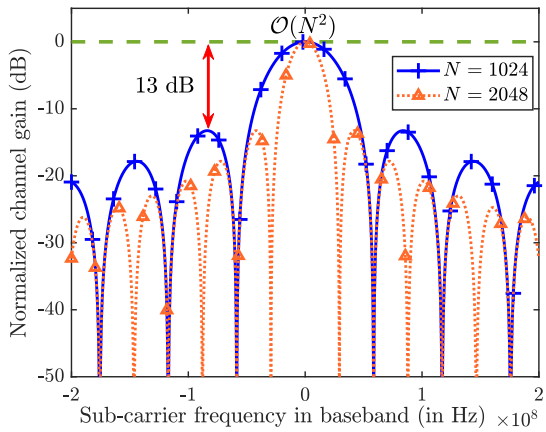

Fig. 2: B-SP effect at $f_c = 30$ GHz, $W = 400$ MHz, $\phi = 90°$.

IRS, the channel coefficient on the kth SC is given in (6). So, the physical angle ϕ of the cascaded channel manifests as

$$\phi_{f_k} = \sin^{-1}_{(p)}\left\{\left(1 + \frac{f_k}{f_c}\right)\sin(\phi)\right\} \tag{7}$$

on the kth SC, which equals ϕ only if $f_k = 0$ or $\phi = 0$. Thus, if the frequency-independent phase shifters at the IRS are tuned at the carrier frequency, $f_k = 0$, i.e., $\boldsymbol{\theta} = \mathbf{a}_N(\phi)$, they can only beamform to ϕ over a small BW around $f_k = 0$ [4] (unless $\phi = 0$.) This results in the *beam-split effect*, and it degrades the array gain on SCs for which $f_k \neq 0$. Further, the B-SP effect is more pronounced at a UE whose cascaded angle is $\phi = 90°$. For e.g., in Fig. 2, we plot the normalized channel gain, $|H[k]|^2$ vs. the SC frequency, f_k when the IRS is tuned to $f_k = 0$. We see that only a few SCs around $f_k = 0$ achieve the full array gain of N^2, while other SCs face a loss of at least 13 dB. In particular, B-SP reduces the array gain to 0, producing deep nulls in the channel gain of SCs at frequencies

$$f_{\text{NULL}} = \frac{2f_c}{N}q, \quad q = \pm 1, \pm 2, \ldots, \pm\left\lfloor \frac{WN}{4f_c} \right\rfloor.$$

Moreover, the B-SP effect is exacerbated when N increases and further reduces the system throughput. In this view, to mitigate the B-SP effect, in this paper, we propose a distributed IRS design using S non-colocated M-element IRSs with $SM = N$ to limit the degradation in the array gain across all SCs. Specifically, the number of IRS elements, M, can be adjusted to control the B-SP effect, and the number of IRSs, S, can be chosen to obtain an array gain of $\mathcal{O}(N^2)$ over the complete BW. Furthermore, in this case, unless the IRSs are positioned appropriately, the signal from each IRS experiences a different propagation delay and leads to a non-zero *temporal delay spread* (TDS) in the overall channel, as shown in Fig. 1(b). Then, we address the following questions.

1) Considering a TDS $= 0$ case, what combinations of (S, M) ensure that the worst-case B-SP results in a loss of no more than $(1-\epsilon)^2$ in the channel gain compared to the peak IRS array gain? That is, we wish to determine $\{(S, M)\}$, the possible pairs (S, M), such that

$$\min_{k\in[K]} |H[k]|^2 \Big|_{\phi_s = 90°} \geq (1-\epsilon)^2 |H[K/2]|^2, \tag{8}$$

where ϕ_s denotes the cascaded angle via IRS-s and $\epsilon \in [0, 1)$ dictates the acceptable loss in array gain relative to the center SC. Here, $\phi_s = 90°$ captures the worst-case B-SP. Note that the condition in (8) ensures that the array gain is within a tolerable residual B-SQ controlled by ϵ.

2) How does the solution perform when multiple IRSs cause a non-zero TDS due to signals from each IRS arriving at the UE at different sampling time instants?

Remark 1. *The B-SP effect arises due to the interplay of using phase shifters and SW effects at the IRS. In particular, phase shifters are effective for compensating the differential delays across the IRS aperture and form a beam only if the narrowband condition, $\Delta\tau \ll 1/W$, is met [31]. However, to retain the low complexity phased array-based IRS architecture for beamforming even in wideband systems, we enforce the narrowband criterion by limiting the number of IRS elements. Since defining the boundary between narrowband and wideband regimes is hard in the time domain, we resolve this by examining the B-SP effect in the frequency domain and ensuring that the narrowband condition is satisfied.*

III. Mitigating Beam-Split Via Distributed IRSs

As discussed, the B-SP effect in the frequency domain arises due to the SW effect caused by the propagation delay across the IRS aperture in the time domain. This can be circumvented if $\Delta\tau^{\text{C}} \ll 1/W$ is satisfied. Given the bandwidth W, this can be ensured by reducing the number of IRS elements. However, this also has the undesirable effect of decreasing the array gain from the IRS and, hence, the throughput. This loss can be avoided by a distributed IRS design, as explained below.

A. Parallelizing the Spatial Delays using Distributed IRSs

The advantage of a distributed design is that it *parallelizes* the spatial delay across the aperture, which otherwise increases *serially* in the number of elements in a large centralized IRS. In particular, partitioning and distributing a single large IRS into multiple non-colocated smaller IRSs reduces the delay across each IRS, i.e., if an N-element IRS is split into S IRSs with M-elements, the delay across the aperture of sth IRS is

$$\Delta\tau^{\text{D}}_s = (M-1)\,(d/c)\,|(\sin(\psi_s) - \sin(\omega_s))| \approx \Delta\tau^{\text{C}}/S, \tag{9}$$

where ψ_s and ω_s denote the DoA and DoD at the sth IRS, respectively. Thus, the delay across the aperture of each IRS is reduced approximately by a factor S, as shown in Fig. 1(b), decreasing the influence of the SW effect. Further, in Sec. V, we also show that distributed IRSs provide angle diversity gains, making it unlikely for the worst-case B-SP to happen at every IRS, further reducing the impact of the B-SP effect.

B. Number of Elements per IRS

We now determine the number of elements per IRS, M, which parallelizes the spatial delay and guarantees (8) for TDS $= 0$ case, and extend it to TDS $\neq 0$ case in Corollary 1.

Theorem 1. *Consider a system with S non-colocated M-element IRSs with a total of N IRS elements (i.e., $SM = N$)*

[4] This holds true even if the IRS is tuned at a different frequency, $f'_k \neq 0$.

with TDS $= 0$. Then, the maximum M for which the array gain due to all IRSs on every SC is at least $(1-\epsilon)^2N^2$ is

$$M^* \triangleq \min\left\{\max\left\{\left\lfloor \frac{4\sqrt{6\epsilon}}{\pi}\frac{f_c}{W}\right\rfloor, 1\right\}, N\right\}, \quad (10)$$

$\epsilon \in [0,1)$ dictates the tolerable loss in array gain w.r.t. N^2.

Proof. We begin the proof by noting that similar to (6), the channel at the UE on SC-k due to S IRSs can be written as

$$H[k] = \sum\nolimits_{s=1}^{S} \sqrt{M}\tilde{h}_s \boldsymbol{\theta}_s^H \mathbf{a}_M\left(\phi_{f_k,s}\right) e^{-j2\pi f_k(\eta_s-\tau_0)}, \quad (11)$$

where $\tilde{h}_s$ is the cascaded channel coefficient via the sth IRS, η_s, τ_0 refer to the propagation delay via the sth IRS, and receiver timing offset, respectively; $\boldsymbol{\theta}_s \in \mathbb{C}^M$ is the phase shift vector at the sth IRS, and $\phi_{f_k,s}$ is the cascaded angle at the UE via the sth IRS on SC-k as given in (7) with ϕ_s being the physical angle via the sth IRS. Since we consider that the TDS is 0, $(\eta_s - \tau_0)W \ll 1$ holds, and hence, we drop the exponential term in (11). Then, by tuning $\boldsymbol{\theta}_s$, $s = 1, \ldots, S$ to the center SC at $f_k = 0$, and by invoking the Cauchy-Schwarz (CS) inequality, we obtain the optimal phase configurations:

$$\boldsymbol{\theta}_s = \sqrt{M}e^{j\angle\tilde{h}_s}\mathbf{a}_M(\phi_s), \ \forall s = 1, \ldots, S, \quad (12)$$

where symbols are defined as above. Substituting (12) in (11), we have

$$|H[k]|^2 = \left|M\sum\nolimits_{s=1}^{S}|\tilde{h}_s|\mathbf{a}_M^H(\phi_s)\mathbf{a}_M\left(\phi_{f_k,s}\right)\right|^2, \quad (13)$$

Now, to account for the worst-case B-SP effect, we use $\phi_s = 90^\circ$ as in (8), and when $M > 1$, we can simplify the channel gain as $|H[k]|^2 =$

$$\left|\sum_{s=1}^{S}|\tilde{h}_s|\frac{1-e^{-j\pi M\frac{f_k}{f_c}}}{1-e^{-j\pi\frac{f_k}{f_c}}}\right|^2 \overset{(a)}{=} M^2\,\mathrm{sinc}^2\left(M\frac{f_k}{2f_c}\right)\left|\sum_{s=1}^{S}|\tilde{h}_s|\right|^2, \quad (14)$$

where, in (a), we use $\sin(x) \approx x$ for $x = \pi f_k/(2f_c) \ll 1$, and $\mathrm{sinc}(x) \triangleq \sin(\pi x)/\pi x$. Clearly, at $f_k = 0$, the response in (14) is maximum and decreases as $f_k \to \pm W/2$. Now using (14), the condition in (8) becomes

$$\min\left\{\mathrm{sinc}^2\left(M\frac{f_k}{2f_c}\right), k = 1, 2, \ldots, K\right\} \geq (1-\epsilon)^2. \quad (15)$$

A necessary condition for (15) to hold is not to have a null response across the entire BW. Since $\mathrm{sinc}^2(x) = 0$ when $x \in \mathbb{Z}$, the set of integers, from (15) we need to satisfy

$$MW/4f_c \leq 1 \implies M \leq M_1^* \triangleq \lfloor 4f_c/W \rfloor. \quad (16)$$

This ensures that the channel response across the BW lies within the main lobe width of the beam formed by the IRS at the center SC. Now, since $\mathrm{sinc}^2(x)$ is a decreasing function for $x \in [0,1]$, a sufficient condition for (15) is

$$|H[0]|^2 = |H[K]|^2 \geq (1-\epsilon)^2|H[K/2]|^2, \text{ i.e.,}$$

$$\mathrm{sinc}^2\left(\pm\frac{MW}{4f_c}\right) \geq (1-\epsilon)^2 \overset{(b)}{\implies} M \leq M_2^* \triangleq \left\lfloor \frac{4\sqrt{6\epsilon}}{\pi}\frac{f_c}{W}\right\rfloor, \quad (17)$$

where in (b), we used the 1st order Taylor's approximation: $\mathrm{sinc}(x) \approx 1 - \pi^2x^2/6$, which is tight in the region of design interest. Now, from (16), and (17), we get

$$M \leq M^* \triangleq \min\{M_1^*, M_2^*\} = M_2^*, \quad (18)$$

where the last step follows because for $\epsilon \in [0,1)$, $M_2^* \leq M_1^*$. Finally, since $1 \leq M \leq N$, we modify (18) as

$$M \leq M_{\text{mod}}^* \triangleq \min\{\max\{M_2^*, 1\}, N\},$$

yielding the desired result in (10). ∎

Therefore, if N is the total number of IRS elements, then deploying at least $S = N/M$ IRSs with M as per Theorem 1 will prevent the adverse impact of the B-SP effect.

C. Sum-Rate Analysis: Centralized vs. Distributed IRSs

In this section, we analyze the achievable sum-rate of the distributed design and also analyze the achievable performance when the channel experiences a nonzero TDS.

In general, the signal arriving at the UE through each IRSs could be time-offset relative to the UE's timing, giving rise to a TDS in the signals arriving through the different IRSs. For analytical tractability, we model the propagation delay via the sth IRS as a random variable, $\tilde{\eta}_s \sim \mathcal{U}[0, T_0]$, independent and identically distributed (i.i.d.) across IRSs. Here, T_0 is the maximum TDS that the IRSs can introduce at the UE's location. We now characterize the achievable sum-rate across SCs at a UE under centralized and distributed IRS scenarios.

Theorem 2. *In an mmWave-OFDM system with K SCs spanning a BW of W at carrier frequency f_c and a total of N IRS elements, the sum-rate at a UE with channel angle ϕ and $\phi_1, \ldots, \phi_S$ under centralized and distributed IRS (with $M = M^*$ as per Theorem 1) setups satisfy*

$$\bar{R}_C \approx \frac{1}{K+N_{CP}^C}\sum_{k=1}^{K}\log_2\left(1+\frac{p_k\sigma_{\text{h}}^2}{\sigma^2}N^2\mathrm{sinc}^2\left(N\frac{f_k}{2f_c}\sin(\phi)\right)\right), \quad (21)$$

and as given in (19)-(20) on top of the next page, respectively, where $\sigma_{\text{h}}^2 = |\tilde{h}|^2 = |\tilde{h}_1|^2 \approx \ldots \approx |\tilde{h}_S|^2$ is the channel gain via the IRSs[5], p_k and σ^2 are the transmit and noise power at the kth SC, and N_{CP}^C, N_{CP}^D are the cyclic prefix (CP) lengths in the centralized and distributed IRS setups,[6] which are respectively

$$N_{CP}^C = \left\lceil (N-1)\frac{W}{f_c}\right\rceil, \ N_{CP}^D = \left\lceil (M-1)\frac{W}{f_c} + WT_0\right\rceil, \quad (22)$$

where T_0 is the maximum TDS induced by the IRSs at a UE.

Proof. In an OFDM system with K SCs, the sum-rate is

$$\bar{R} \triangleq \mathbb{E}_{\{H[k]\}_{k=1}^K}\left[\frac{1}{K+N_{\text{CP}}}\sum_{k=1}^{K}\log_2\left(1+\frac{p_k}{\sigma^2}|H[k]|^2\right)\right]$$

[5]We consider equal path losses in the paths across all IRSs only for the sake of analysis and to present how the performance scales with the number of IRSs and IRS elements. Our solution is applicable even when path losses are unequal among the cascaded links through each IRS.

[6]The CP in OFDM is used to (a) eliminate inter-symbol interference, and (b) convert the linear convolution with a frequency-selective channel into circular convolution, which diagonalizes the channel in the frequency domain. However, this does not eliminate the SW effect itself. Specifically, large IRS apertures cause significant delay spreads, which result in the B-SP effect with SC-dependent channel variations as shown in Fig. 2. The gain on a given SC is still governed by the time-domain channel's impulse response via a Fourier transform. Thus, while CP simplifies OFDM-based signal processing, it does not mitigate the SW-induced B-SP effects inherent to large IRSs.

$$\bar{R}_{\mathrm{D}} \geq \mathsf{R}_{\min} \triangleq \frac{1}{K+N_{\mathrm{CP}}^{\mathrm{D}}} \sum_{k=1}^{K} \log_2\left(1+\frac{p_k\sigma_{\mathrm{h}}^2}{\sigma^2} M^2\left(1-\epsilon\right)^2\left[S^2\,\mathrm{sinc}^2(f_kT_0)+S\left(1-\mathrm{sinc}^2(f_kT_0)\right)\right]\right), \tag{19}$$

$$\geq \mathsf{R}_{\min}^{\text{L-bound}} \triangleq \frac{1}{K+N_{\mathrm{CP}}^{\mathrm{D}}} \sum_{k=1}^{K} \log_2\left(1+\frac{p_k\sigma_{\mathrm{h}}^2}{\sigma^2} SM^2\left(1-\epsilon\right)^2\right), \tag{20}$$

$$\overset{(a)}{\approx} \frac{1}{K+N_{\mathrm{CP}}} \sum\nolimits_{k=1}^{K} \log_2\left(1+\frac{p_k}{\sigma^2}\mathbb{E}\left[|H[k]|^2\right]\right), \tag{23}$$

where in (a), we used the Jensen's approximation. We next compute $\mathbb{E}\left[|H[k]|^2\right]$ for centralized & distributed IRSs below:

Centralized scenario: The channel gain for a centralized scenario can be found using (14) with $M=N$, $S=1$. Then,

$$\mathbb{E}\left[|H[k]|^2\right] = N^2\,\mathrm{sinc}^2\left(N\frac{f_k}{2f_c}\sin(\phi)\right)\underbrace{\mathbb{E}[|\tilde{h}|^2]}_{=\sigma_{\mathrm{h}}^2}, \tag{24}$$

and substituting the above into (23) yields (21).

Distributed scenario: Let $\tilde{\eta}_s \triangleq \eta_s - \tau_0$ be the propagation delay of the path via the sth IRS w.r.t the timing offset at the UE. Since $(\eta_s-\tau_0)W \ll 1$ may not hold in general, from (11), the channel gain at a UE on SC-k is given by

$$|H[k]|^2 = \left|M\sum\nolimits_{s=1}^{S}|\tilde{h}_s|\mathbf{a}_M^H(\phi_s)\mathbf{a}_M\left(\phi_{f_k,s}\right)e^{-j2\pi f_k\tilde{\eta}_s}\right|^2.$$

Similar to (14), the expected channel gain is $\mathbb{E}\left[|H[k]|^2\right] =$

$$\mathbb{E}\left[\left|\sum\nolimits_{s=1}^{S}|\tilde{h}_s|\frac{1-e^{-j\pi M\frac{f_k}{f_c}\sin(\phi_s)}}{1-e^{-j\pi\frac{f_k}{f_c}\sin(\phi_s)}}e^{-j2\pi f_k\tilde{\eta}_s}\right|^2\right] \tag{25}$$

$$\overset{(b)}{\geq} M^2\,\mathrm{sinc}^2\left(M\frac{f_k}{2f_c}\right)\mathbb{E}\left[\left|\sum\nolimits_{s=1}^{S}|\tilde{h}_s|e^{-j2\pi f_k\tilde{\eta}_s}\right|^2\right], \tag{26}$$

where in (b), we applied the result from Theorem 1. We now simplify the above expectation term as

$$\mathbb{E}\left[\left|\sum\nolimits_{s=1}^{S}|\tilde{h}_s|e^{-j2\pi f_k\tilde{\eta}_s}\right|^2\right] = \sum\nolimits_{s=1}^{S}|\tilde{h}_s|^2 + \sum_{s=1}^{S}\sum_{\substack{s'=1\\ s\neq s'}}^{S}|\tilde{h}_s||\tilde{h}_{s'}|\mathbb{E}\left[e^{-j2\pi f_k\tilde{\eta}_s}\right]\mathbb{E}\left[e^{j2\pi f_k\tilde{\eta}_{s'}}\right]. \tag{27}$$

Next, we compute $\mathbb{E}\left[e^{j2\pi f_k\tilde{\eta}_s}\right]$ as shown below.

$$\mathbb{E}\left[e^{j2\pi f_k\tilde{\eta}_s}\right] = \frac{1}{T_0}\int_0^{T_0} e^{j2\pi f_k\eta}\mathrm{d}\eta = \frac{1}{T_0}\frac{e^{j2\pi f_k\eta}}{j2\pi f_k}\Bigg|_0^{T_0}$$
$$= \frac{1}{T_0}\frac{e^{j\pi f_kT_0}\left(e^{j\pi f_kT_0}-e^{-j\pi f_kT_0}\right)}{j2\pi f_k}$$
$$= e^{j\pi f_kT_0}\cdot\frac{\sin\left(\pi f_kT_0\right)}{\pi f_kT_0} = e^{j\pi f_kT_0}\,\mathrm{sinc}\left(f_kT_0\right). \tag{28}$$

Similarly, we can show that

$$\mathbb{E}\left[e^{-j2\pi f_k\tilde{\eta}_s}\right] = e^{-j\pi f_kT_0}\,\mathrm{sinc}\left(f_kT_0\right). \tag{29}$$

Using (28) and (29) in (27), we get

$$\mathbb{E}\left[\left|\sum_{s=1}^{S}|\tilde{h}_s|e^{-j2\pi f_k\tilde{\eta}_s}\right|^2\right] = S\sigma_{\mathrm{h}}^2 + S(S-1)\sigma_{\mathrm{h}}^2\,\mathrm{sinc}^2\left(f_kT_0\right)$$
$$= \sigma_{\mathrm{h}}^2\left(S^2\,\mathrm{sinc}^2(f_kT_0)+S(1-\mathrm{sinc}^2(f_kT_0))\right).$$

Now, using the above in (26), and by Theorem 1, we obtain

$$\mathbb{E}\left[|H[k]|^2\right] \geq (1-\epsilon)^2M^2\sigma_{\mathrm{h}}^2\left(S^2\,\mathrm{sinc}^2(f_kT_0) + S(1-\mathrm{sinc}^2(f_kT_0))\right). \tag{30}$$

Substituting (30) in (23) and by the monotonicity of $\log(\cdot)$, (19) follows. We get (20) by the lower bound of the convex combination, i.e., $S^2\,\mathrm{sinc}^2(f_kT_0)+S(1-\mathrm{sinc}^2(f_kT_0)) \geq S$.

Next, note that the CP lengths should exceed the channel delay spread. The delay spread, τ under centralized and distributed IRSs are $\Delta\tau^{\mathrm{C}}$ from (4), and $\max_{s\in[S]}\left\{\Delta\tau_s^{\mathrm{D}}+\tilde{\eta}_s\right\}$ from (9), respectively. In particular, the CP length in the distributed IRS case should account for the residual spatial delay spread and the temporal delay spread introduced by the multiple IRSs. Then, using these expressions in the length of discrete-time channel taps: $N_{\mathrm{CP}} = \lceil W\tau\rceil$, we get

$$N_{\mathrm{CP}}^{\mathrm{C}} = \left\lceil (N-1)\frac{W}{2f_c}\Delta S^{\mathrm{C}}\right\rceil, \quad \text{and}$$
$$N_{\mathrm{CP}}^{\mathrm{D}} = \left\lceil \max_{1\leq s\leq S}\left\{(M-1)\frac{W}{2f_c}\Delta S_s^{\mathrm{D}} + W\tilde{\eta}_s\right\}\right\rceil,$$

respectively, where $\Delta S^{\mathrm{C}} \triangleq |\sin(\psi)-\sin(\omega)|$, $\Delta S_s^{\mathrm{D}} \triangleq |\sin(\psi_s)-\sin(\omega_s)|$. Now, to satisfy the CP requirements at any UE, we upper bound the delays and set $\Delta S^{\mathrm{C}} = \Delta S^{\mathrm{D}} = 2$, and $\tilde{\eta}_s = T_0$. Then the desired CP lengths in (22) follow. ■

From Theorem 2, we observe that unlike a centralized scenario, which results in zero rates on many SCs, the distributed IRS provides a positive rate that scales at least as much as $\mathcal{O}(\log(SM^2))$ on all SCs which guarantees a lower bound on the sum-rate given by $R_{\min}^{\text{L-bound}}$ in (20). Hence, distributed IRSs can effectively mitigate the SW and the resulting B-SP effects in the system under any circumstance. We also make the following observations from this theorem:

1) Effect of nonzero TDS on the number of IRS elements, M^*: Even in the presence of non-zero TDS in the overall channel at the UE, our design based on Theorem 1 ensures that SW effect gets mitigated. We formalize this in the following.

Corollary 1. *For a distributed IRS system having a finite TDS, the value of M given by Theorem 1 still mitigates the B-SP in the sense of procuring an array gain which is at least $(1-\epsilon)^2$ factor of the peak array gain obtained on SCs around $f_k = 0$.*

Proof. When the TDS is non-negligible, we set $\phi_1 = \phi_2 = \ldots = \phi_S = 90°$ in (25) to capture the worst case B-SP and obtain the simplified channel gain on SC-k as

$$|H[k]|^2 = M^2\,\mathrm{sinc}^2\left(M\frac{f_k}{2f_c}\right)\left|\sum\nolimits_{s=1}^{S}|\tilde{h}_s|e^{-j2\pi f_k\tilde{\eta}_s}\right|^2. \tag{31}$$

Next, using (31), the condition in (8) can be simplified as

$$\mathrm{sinc}^2\left(M\frac{f_k}{2f_c}\right) \geq (1-\epsilon)^2\left|\sum_{s=1}^{S}|\tilde{h}_s|\right|^2 \Big/ \left|\sum_{s=1}^{S}|\tilde{h}_s|e^{-j2\pi f_k\tilde{\eta}_s}\right|^2$$

$$\overset{(a)}{\geq} (1-\epsilon)^2 \frac{\left|\sum_{s=1}^{S} |\tilde{h}_s|\right|^2}{S\sum_{s=1}^{S}|\tilde{h}_s|^2} \overset{(b)}{=} (1-\epsilon)^2 \left\|\tilde{\mathbf{h}}\right\|_1^2 \Big/ S\left\|\tilde{\mathbf{h}}\right\|_2^2, \quad (32)$$

where (a) follows by the CS inequality, and in (b), we define $\tilde{\mathbf{h}} \triangleq [|\tilde{h}_1|, \ldots, |\tilde{h}_S|]^T$. Since $\|\tilde{\mathbf{h}}\|_1 \leq \sqrt{S}\|\tilde{\mathbf{h}}\|_2$ [32], a sufficient condition for (32) becomes that given in (15), and hence rest of the proof follows similar to TDS $= 0$ case. ■

Fundamentally, the TDS does not affect the value of M used to mitigate the B-SP effects. This is because by controlling M, we directly tune the tolerable spatial delay at each IRS, which is independent of the presence and location of other IRSs.

2) Channel gain via distributed IRSs: Although the distributed IRSs provide (an almost) flat response over the entire BW, this flat gain can go as low as $\mathcal{O}(SM^2)$. In particular,

(a) From (19), the (flat) gain is dictated by M and the convex combination, $S^2\,\mathrm{sinc}^2(f_kT_0) + S(1-\mathrm{sinc}^2(f_kT_0))$:
- If $T_0 \ll 1/W$, then $\mathrm{sinc}(f_kT_0) \approx 1$ on all SCs, ensuring a array gain of $S^2M^2 = N^2$ on all SCs.
- If $T_0 \gtrsim 1/W$, then $\mathrm{sinc}(f_kT_0) \approx 0$ around the band-edge frequencies. Then, an array gain of at least SM^2 is obtained over the BW of the operation.
- If $f_k = 0$, $\mathrm{sinc}(f_kT_0) = 1$ for any T_0, and a full array gain of N^2 is obtained. This is because when the IRS is tuned to the center frequency: $f_k = 0$, for any T_0, there exists a smaller BW around $f_k = 0$, in which the IRS phase shifts can always compensate for the differential delays across the IRSs, yielding the array gain of N^2.

(b) From the above, the locations of the IRSs are important:
- If the locations of IRSs are such that $T_0 \ll 1/W$, then TDS ≈ 0, and the signals from IRSs can coherently add at the UE, giving $\mathcal{O}(N^2)$ gain on all SCs.
- If the IRSs are positioned such that they introduce a finite TDS, then the IRSs whose propagation delays are within the same sampling interval constructively add the signals at the UE, and the IRSs whose propagation delays fall at different sampling bins incoherently add the signals at the UE. This gives rise to a channel gain fluctuation between $\mathcal{O}(SM^2)$ and $\mathcal{O}(N^2)$.
- Finally, if the IRSs are positioned such that the propagation delays of each IRS fall on distinct sampling bins, giving rise to larger TDS, the signals from different IRSs do not coherently superimpose at the UE, leading to an incoherent channel gain that scales as $\mathcal{O}(SM^2)$.

In summary, a distributed IRS design:

1) overcomes the SW effect in IRS-aided wideband systems *without any deep-nulls* in the channel gain at the UE, and
2) results in an almost flat response whose gain varies as
$$\forall k \in [K] : \mathcal{O}(SM^2) \leq |H[k]|^2 \leq \mathcal{O}(S^2M^2 = N^2),$$
depending on the relative location of IRSs and the TDS.

Remark 2 (Choice of ϵ)**.** *The parameter ϵ in Theorems 1, 2 which captures the tolerable loss in the array gain across SCs is the designer's choice; a few suggestions are given below.*

1) The spatial range in the half-power beam width (HPBW) procures most of the array gain of the IRS [33]. So, setting $\epsilon = 1 - \frac{1}{\sqrt{2}}$ ensures that the HPBW of each IRS spans full BW at a UE. Then, the signal lies within the HPBW of a virtual array with $N = SM$ elements if the TDS is small.

2) In the 5G NR setting, all SCs are alloted the same modulation & coding scheme index (MCSI) [34]. Then, an ϵ that maps the spectral efficiencies of all SCs to the same MCSI can be chosen to reap the full achievable throughput.

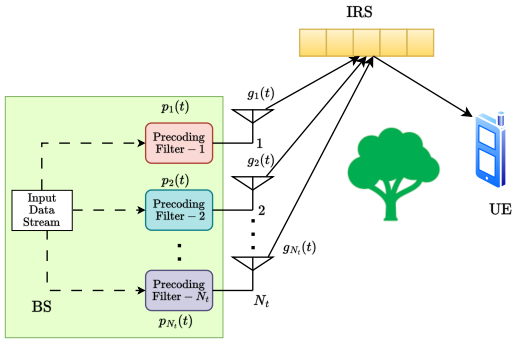

Fig. 3: System with multiple-antenna BS.

Remark 3. *Our solution to mitigate the SW effect applies to any IRS geometry. In particular, the aperture length, measuring the farthest distance between two IRS elements, determines the impact of the SW effect. For instance, for a uniform planar array (UPA) based IRS, the number of elements in Theorem 1 corresponds to the number of diagonal elements of the UPA. We numerically illustrate the performance of our solution under a UPA configuration in Fig. 7.*

Further, when the number of IRSs increases, the number of IRS controllers also increases in the system. On the other hand, one can still use low-pilot overhead channel estimation algorithms with multiple IRSs, as given in [35].

D. Extension to Multiple-antenna Systems

We now extend our solution to a multi-antenna BS scenario; the approach can be easily adapted to the setup where the UEs are also equipped with multiple antennas. We consider an N_t-element ULA at a BS serving a UE via an N-element IRS over a bandwidth W, as shown in Fig. 3. Let $p_m(t)$ denote the precoding filter at the mth BS antenna, and $g_m(t)$ be the cascaded channel between the mth antenna and the UE, for $m \in [N_t]$. Following the same steps as in (3), we obtain

$$g_m(t) = \sum\nolimits_{n=1}^{N} \theta_n \tilde{h}_{1,m}\tilde{h}_2 \delta\Big(t - \eta_m - (n-1)\frac{d}{c} \times (\sin(\psi) - \sin(\omega))\Big) e^{-j2\pi f_c(n-1)\frac{d}{c}\sin(\phi)}, \quad (33)$$

where $\tilde{h}_{1,m} = \sqrt{\alpha}e^{-j2\pi f_c \eta_m^{(1)}}$ with $\eta_m^{(1)}$ being the propagation delay from the mth BS antenna to a reference IRS element, and η_m $(= \eta_m^{(1)} + \eta^{(2)})$ is the total propagation delay from the mth antenna to the UE via the reference element of the IRS. By using the properties of the ULA, we can express $\eta_m^{(1)}$ as

$$\eta_m^{(1)} = \eta^{(1)} + (m-1)\frac{d_{\mathrm{BS}}}{c}\sin(\varrho), \quad (34)$$

where $\eta^{(1)}$ is the delay from the reference BS antenna to the reference IRS element, d_{BS} is the inter-antenna spacing at the BS, and ϱ is the DoD of the signal at the BS. Then, we simplify (33) and obtain the expression in (35), where η and $\tilde{h}_1$ are defined as given in (3). From (35), the overall channel

$$g_m(t) = \sum_{n=1}^{N} \theta_n \tilde{h}_1 \tilde{h}_2 \delta\left(t - \eta - (m-1)\frac{d_{\text{BS}}}{c}\sin(\varrho) - (n-1)\frac{d}{c}\left(\sin(\psi) - \sin(\omega)\right)\right) e^{-j2\pi f_c\left((m-1)\frac{d_{\text{BS}}}{c}\sin(\varrho)+(n-1)\frac{d}{c}\sin(\phi)\right)}. \tag{35}$$

$$h(t) = \sum\nolimits_{n=1}^{N} \theta_n \tilde{h}_1 \tilde{h}_2 \sum\nolimits_{m=1}^{N_t} \delta\left(t - \eta - (m-1)\frac{d_{\text{BS}}}{c}\sin(\varrho) - (n-1)\frac{d}{c}\left(\sin(\psi) - \sin(\omega)\right) - \tau_{m,\text{BS}}\right) \times e^{j\phi_{m,\text{BS}}} \times e^{-j2\pi f_c\left((m-1)\frac{d_{\text{BS}}}{c}\sin(\varrho)+(n-1)\frac{d}{c}\sin(\phi)\right)}. \tag{38}$$

experiences a *two-tier* B-SP effect, one originating from the IRS and the other from the BS array—due to SW effects at both ends. However, since the BS is not as constrained by power and hardware limitations, it is practically feasible to equip each antenna with a TTD unit, enabling effective compensation for the SW and the resulting B-SP effect at the BS. Accordingly, the impulse response of the precoding filter at the mth antenna is given by [20]

$$p_m(t) = e^{j\phi_{m,\text{BS}}}\delta\left(t - \tau_{m,\text{BS}}\right), \tag{36}$$

where $\phi_{m,\text{BS}}$ and $\tau_{m,\text{BS}}$ denote the phase and delay applied at the mth antenna. Then, the (precoded) effective channel is

$$h(t) = \sum\nolimits_{m=1}^{N_t} g_m(t) \circledast p_m(t). \tag{37}$$

Substituting $g_m(t)$ and $p_m(t)$ from (35) and (36) into (37), we obtain the effective channel expression in (38). To mitigate the B-SP effect, we configure the TTD units as follows:

$$\tau_{m,\text{BS}} = \tau_{0,\text{BS}} - (m-1)\frac{d_{\text{BS}}}{c}\sin(\varrho), \text{ and} \tag{39}$$

$$\phi_{m,\text{BS}} = 2\pi f_c (m-1)\frac{d_{\text{BS}}}{c}\sin(\varrho), \tag{40}$$

where $\tau_{0,\text{BS}}$ is a common delay applied at all the antenna elements to ensure a causal implementation of the TTDs at the BS array. As a result, the effective channel boils down to

$$h(t) = N_t \sum\nolimits_{n=1}^{N} \theta_n \tilde{h}_1 \tilde{h}_2 \delta\left(t - \eta - \tau_{0,\text{BS}} - (n-1)\frac{d}{c} \times \left(\sin(\psi) - \sin(\omega)\right)\right) \times e^{-j2\pi f_c (n-1)\frac{d}{c}\sin(\phi)}, \tag{41}$$

which is a scaled version of the channel with a single-antenna BS (as in (3)), except for an extra timing offset of $\tau_{0,\text{BS}}$, with the scaling factor equal to the number of BS antennas.

Thus, the results developed in this paper identically hold when the BS is equipped with multiple antennas also.

IV. Optimizing the Locations of Distributed IRSs

From the preceding discussions, we further make the following crucial observations. For a channel with a large TDS,

- The achievable channel gain flattens at $\mathcal{O}(SM^2)$, with a loss of $10\log_{10}(S)$ dB from the maximum gain of $\mathcal{O}(N^2)$,
- The required length of the CP increases linearly with the TDS, increasing the OFDM overheads with many IRSs.

As a consequence, selecting arbitrary locations for the IRSs results in diminished performance compared to the maximum achievable performance (for e.g., the array gain that scales as N^2 on all SCs), despite its benefit in alleviating the SW effect and preventing deep nulls in the channel response. Thus, we now shift our focus to optimizing the placement of the IRSs to minimize the resulting TDS in the system.

Optimizing the locations of IRSs is critically dependent on the positions of both the UE and the BS. Further, in general, the BS serves multiple non-colocated UEs, especially in densely populated hotspot scenarios where IRSs are used to enhance service quality [36]. In such cases, determining the IRS locations based on a single UE's location may be suboptimal. However, since the optimization of the IRS locations with multiple UEs makes the problem intractable, we first focus on optimizing IRS locations for a single UE, gain insights; then analyze the scenario for multiple UEs.

A. Optimizing the Locations of IRSs For a Single User

Without loss in generality, let the BS be located at $\mathbf{0} \triangleq [0,0]^T$ on the x-y plane. Let the location of the UE be $\mathbf{p} \triangleq [p_1, p_2]^T \in \mathbb{R}^2$, and the location of IRSs be $\mathcal{Q} = \{\mathbf{q}_1, \mathbf{q}_2, \ldots, \mathbf{q}_S\}$, where $\mathbf{q}_s \in \mathbb{R}^2$. Then, define the following:

$$T_{\max}(\mathcal{Q}) = \max_{1\le s\le S} \left(\|\mathbf{q}_s\|_2 + \|\mathbf{p} - \mathbf{q}_s\|_2\right)/c, \tag{42}$$

$$T_{\min}(\mathcal{Q}) = \min_{1\le s\le S} \left(\|\mathbf{q}_s\|_2 + \|\mathbf{p} - \mathbf{q}_s\|_2\right)/c, \tag{43}$$

the maximum and minimum propagation delays from BS to the UE via the IRSs. The TDS in the BS-UE channel is

$$T_d^{\text{D}}(\mathcal{Q}) \triangleq T_{\max}(\mathcal{Q}) - T_{\min}(\mathcal{Q}).$$

Then, the locations of the IRSs can be found as

$$\mathcal{Q}^* \triangleq \{\mathbf{q}_1^*, \mathbf{q}_2^*, \ldots, \mathbf{q}_S^*\} = \arg\min_{\mathbf{q}_1,\ldots,\mathbf{q}_S} T_d^{\text{D}}(\mathcal{Q}). \tag{P1}$$

We have the following result that solves the problem in (P1).

Theorem 3. *When BS and UE are located at points* $\mathbf{0}$ *and* $\mathbf{p}$*, respectively, the optimal locations of IRSs* $(\mathbf{q}_1^*, \ldots, \mathbf{q}_S^*)$ *as the solution to* (P1) *satisfy the equation:*

$$g_{\lambda,\mathbf{p}}(\mathbf{q}) \triangleq \left\|\mathbf{R}_{\omega,\mathbf{p}}^{\lambda}\left(\mathbf{q} - \frac{\mathbf{p}}{2}\right)\right\|_2^2 - 1 = 0, \tag{44}$$

where we define $\omega \triangleq \tan^{-1}\left(\frac{p_2}{p_1}\right)$*, and*

$$\mathbf{R}_{\omega,\mathbf{p}}^{\lambda} \triangleq \begin{bmatrix} \frac{2\cos(\omega)}{\lambda} & \frac{2\sin(\omega)}{\lambda} \\ \frac{2\sin(\omega)}{\sqrt{\lambda^2 - \|\mathbf{p}\|_2^2}} & -\frac{2\cos(\omega)}{\sqrt{\lambda^2 - \|\mathbf{p}\|_2^2}} \end{bmatrix}, \tag{45}$$

with $\lambda \in \mathbb{R}_+$ *being a constant satisfying* $\lambda > \|\mathbf{p}\|_2$*. Further, when the points in* $\mathcal{Q}$ *satisfy* (44)*, the optimal TDS is* $T_d^{D^*} = 0$.

Proof. By their definitions, we note that $T_{\max}(\mathcal{Q}) \geq T_{\min}(\mathcal{Q}) \geq 0$ for all $\mathcal{Q} \subset \mathbb{R}_S^2 \triangleq \underbrace{\mathbb{R}^2 \times \ldots \times \mathbb{R}^2}_{S \text{ times}}$. In other words, $T_d^{\mathrm{D}*} = 0$ is the global minimum of the problem: $\min_{\mathcal{Q} \subset \mathbb{R}_S^2} T_d^{\mathrm{D}}(\mathcal{Q})$, and is achieved by a $\mathcal{Q}^*$ for which $T_{\max}(\mathcal{Q}^*) = T_{\min}(\mathcal{Q}^*)$. Thus, the possible global optimal set of IRS locations, $\mathcal{Q}^*$, should be such that $\|\mathbf{q}_s\|_2 + \|\mathbf{p} - \mathbf{q}_s\|_2 = \lambda$ for all $s \in [S]$ and λ is some constant. In other words, the sum-distance of the IRS from the BS and UE should be constant across the IRS locations. Now, using [37, Page 2], it can be shown that an ellipse with the focal points coinciding with the locations of BS and UE satisfies this property. Hence, the IRSs should lie on an ellipse constructed with the BS and UE as foci. Particularly, the equation of the ellipse is

$$\frac{\left((q_1 - q_{10})\cos(\omega) + (q_2 - q_{20})\sin(\omega)\right)^2}{a^2} + \frac{\left((q_1 - q_{10})\sin(\omega) - (q_2 - q_{20})\cos(\omega)\right)^2}{b^2} = 1, \quad (46)$$

where $\mathbf{q} = [q_1, q_2]^T$ is a candidate IRS location, $\mathbf{q}_0 = [q_{10}, q_{20}]^T$ is the center of the ellipse, ω is the angle made by the major axis of ellipse with the x-axis, a and b are lengths of the semi-major axis and semi-minor axis, respectively. Now, with focal points given by $\mathbf{0}$ and $\mathbf{p}$, the centre of the ellipse is $\mathbf{q}_0 = \mathbf{p}/2$. Similarly, using the properties of the ellipse, we can show $a = \lambda/2$, $b = \sqrt{\lambda^2 - \|\mathbf{p}\|_2^2}/2$,[7] and $\omega = \tan^{-1}(p_2/p_1)$, with $\mathbf{p} = [p_1, p_2]^T$. Using these values in (46) and compactly representing it through (44) completes the proof. ∎

From Theorem 3, we note that for a point-point system, the geometric locus of all optimal IRS locations belongs to a family of confocal ellipses, with the BS and UE located at their foci. Specifically, we can choose any $\lambda > \|\mathbf{p}\|_2$, as per the required distance between the BS/UE and IRSs, and find S distinct solutions to (44); these provide a set of IRS locations that solve (P1). Then, the TDS can be avoided entirely (i.e., $T_0 = 0$ in (19)), in turn ensuring the maximum array gain scaling of $\mathcal{O}(N^2)$ on all SCs.

More intuitively, a centralized IRS leads to a non-negligible spatial delay spread in the channel, causing the SW effects. On the other hand, a distributed IRS splits a single IRS into several non-colocated IRSs with fewer elements each that are placed on the circumference of an ellipse, as described in Theorem 3. This ensures that the IRSs do not cause significant spatial or temporal delay spread, resulting in a nearly flat response over the full BW at the peak array gain.

B. Performance with Multiple Users

Note that Theorem 3 cannot be used to determine the IRS locations that are jointly optimal to multiple UEs because:

1) Unless the UEs are colocated, the locations given by (44) are not optimal to all the UEs, i.e., no single solution exists for IRS locations so that the TDS in the channels at all UEs can simultaneously be minimized to $T_d^{\mathrm{D}*} = 0$.
2) Even if the optimization problem in (P1) is solved for each scheduled UE, the solutions are not practically realizable because the locations of IRSs are typically fixed once deployed and do not change with time.

[7]Note that, by applying the triangle inequality property to the triangle formed by BS, UE, and an IRS, it holds that $\lambda > \|\mathbf{p}\|_2$.

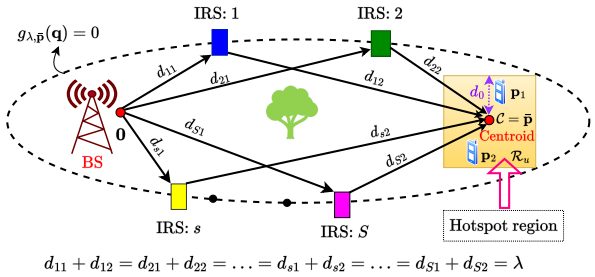

Fig. 4: Geometric locus of IRS locations in the presence of multiple UEs.

To that end, we adopt a reasonable choice of IRS locations that minimize the TDS across all the UEs, as explained next.

We consider a scenario where the BS serves multiple UEs located in a small square hotspot region, $\mathcal{R}_u$, assisted by the distributed IRSs. In this case, a metric of interest is the TDS computed using the propagation delays averaged over the distribution of UE locations within the hotspot area. The expected value of the propagation delay of a path from the BS to UE via an IRS placed at $\mathbf{q}$ is

$$\bar{\tau}(\mathbf{q}) = \mathbb{E}_{\mathbf{p} \sim \mathrm{f}_\mathbf{p}} \left[\|\mathbf{q}\|_2 + \|\mathbf{p} - \mathbf{q}\|_2\right]/c,$$

where $\mathbf{p}$ and $\mathrm{f}_\mathbf{p}$ denote the UE location and its distribution, respectively. We now make the following observation:

$$\mathbb{E}_{\mathbf{p} \sim \mathrm{f}_\mathbf{p}} \left[\|\mathbf{q}\|_2 + \|\mathbf{p} - \mathbf{q}\|_2\right] \approx \|\mathbf{q}\|_2 + \|\mathbb{E}_{\mathbf{p} \sim \mathrm{f}_\mathbf{p}}[\mathbf{p}] - \mathbf{q}\|_2, \quad (47)$$

where we used the Jensen's approximation over the convex $\|\cdot\|_2$ norm. Note that this approximation is accurate when the sum-variance of the components of $\mathbf{p}$ is small, e.g., when the UEs are clustered in a hotspot region around a central point, as is the case in typical IRS deployments [36]. Now, using (47) yields propagation delays via the IRSs similar to (42) and (43), except that the UE location, $\mathbf{p}$, is replaced by the centroid of the distribution of the UE locations, $\bar{\mathbf{p}} \triangleq \mathbb{E}_{\mathbf{p} \sim f_\mathbf{p}}[\mathbf{p}]$. Thus, Theorem 3 can be re-used for multiple UEs also: when multiple UEs are randomly distributed in a hotspot zone, a pragmatic choice of IRS locations is to place them on an ellipse with foci at BS and $\mathcal{C} = \mathbb{E}[\mathbf{p}]$, the *centroid* of the UE distribution, $f_\mathbf{p}(\mathbf{p}), \mathbf{p} \in \mathcal{R}_u$, as shown in Fig. 4. Then, a natural question is: what is the TDS at a UE arbitrarily located in the hotspot area? We have the following result.

Proposition 1. *Consider S distributed IRSs with M elements each, such that the IRSs are positioned at $\mathbf{q}_1, \mathbf{q}_2, \ldots, \mathbf{q}_S$ which lie on ellipse whose focal points are given by the locations of the BS and the centroid, $\bar{\mathbf{p}}$ (i.e., the IRS locations satisfy $g_{\lambda,\bar{\mathbf{p}}}(\mathbf{q}) = 0$ in (44), for some λ satisfying $\lambda > \|\bar{\mathbf{p}}\|_2$.) Then the TDS at a UE located within the hotspot at a distance r (in meters) from the centroid, and at an angle φ, measured anticlockwise w.r.t. the major axis of the ellipse, is*

$$\Delta\tau = \frac{2r}{c} \sin\left(\varphi + \frac{\nu_{\bar{S}} + \nu_{\bar{s}}}{2}\right) \sin\left(\frac{\nu_{\bar{s}} - \nu_{\bar{S}}}{2}\right), \quad (48)$$

where $\nu_s \triangleq \sin^{-1}\left(\frac{\|\mathbf{q}_s\|_2}{\|\mathbf{q}_s - \bar{\mathbf{p}}\|_2} \sin(\chi_s)\right)$, $c = 3 \times 10^8$ *m/s,*

$$\bar{S} \triangleq \arg \max_{1 \leq s \leq S} r\cos(\nu_s + \varphi), \quad \bar{s} \triangleq \arg \min_{1 \leq s \leq S} r\cos(\nu_s + \varphi),$$

and $\chi_s \triangleq \tan^{-1}\left(\frac{[\mathbf{q}_s]_2}{[\mathbf{q}_s]_1}\right) - \tan^{-1}\left(\frac{[\bar{\mathbf{p}}]_2}{[\bar{\mathbf{p}}]_1}\right)$.

Proof. To measure the TDS at an arbitrary UE located at (say) $\mathrm{A}(\mathbf{p})$, we first compute the total propagation delay of the signal from the BS to A via the sth IRS. For convenience, we label the locations of the BS, IRS-s, and centroid by F_1, I_s, F_2, respectively, as shown in Fig. 5. For the triangle $\mathrm{I}_s\mathrm{A}\mathrm{F}_2$, we apply the cosine rule [38, Sec. 12.7] to obtain

$$\mathsf{d}(\mathrm{I}_s,\mathrm{A})^2 = \mathsf{d}(\mathrm{I}_s,\mathrm{F}_2)^2 + \mathsf{d}(\mathrm{F}_2,\mathrm{A})^2 - 2\mathsf{d}(\mathrm{I}_s,\mathrm{F}_2)\cdot\mathsf{d}(\mathrm{F}_2,\mathrm{A})\cos(\Omega_s), \tag{49}$$

where $\mathsf{d}(\mathrm{A},\mathrm{B})$ measures the distance between points A and B, and Ω_s is the angle between the lines $\mathrm{I}_s\mathrm{F}_2$ and $\mathrm{A}\mathrm{F}_2$. Using (49), we make the following simplifications:

$$\begin{aligned}
&\mathsf{d}(\mathrm{I}_s,\mathrm{A}) = \sqrt{\mathsf{d}(\mathrm{I}_s,\mathrm{F}_2)^2 + r^2 - 2r\cdot\mathsf{d}(\mathrm{I}_s,\mathrm{F}_2)\cos(\Omega_s)} \\
&= \sqrt{\mathsf{d}(\mathrm{I}_s,\mathrm{F}_2)^2\left(1 + \frac{r^2}{\mathsf{d}(\mathrm{I}_s,\mathrm{F}_2)^2} - 2\frac{r}{\mathsf{d}(\mathrm{I}_s,\mathrm{F}_2)}\cos(\Omega_s)\right)} \\
&\overset{(a)}{=} \mathsf{d}(\mathrm{I}_s,\mathrm{F}_2)\left(1 - \frac{r}{\mathsf{d}(\mathrm{I}_s,\mathrm{F}_2)}\cos(\Omega_s) + \mathcal{O}\left(\frac{r^2}{\mathsf{d}(\mathrm{I}_s,\mathrm{F}_2)^2}\right)\right) \\
&\overset{(b)}{\approx} \mathsf{d}(\mathrm{I}_s,\mathrm{F}_2) - r\cos(\Omega_s) \overset{(c)}{=} \mathsf{d}(\mathrm{I}_s,\mathrm{F}_2) + r\cos(\nu_s+\varphi),
\end{aligned}$$

where in (a), we used Taylor's expansion: $\sqrt{1+x} = 1 + x/2 + \mathcal{O}(x^2)$; in (b), we neglected higher order terms because the UEs are clustered in a hotspot, i.e., $r \ll \mathsf{d}(\mathrm{I}_s,\mathrm{F}_2)$; and in (c), we used the fact $\varphi + \Omega_s + \nu_s = \pi$ and $\cos(\pi-\theta) = -\cos(\theta)$. As a result, the total propagation delay in the channel at the UE from BS via the sth IRS can be written as $\tau_s^{\mathrm{A}} =$

$$\frac{\mathsf{d}(\mathrm{F}_1,\mathrm{I}_s) + \mathsf{d}(\mathrm{I}_s,\mathrm{A})}{c} \approx \frac{\mathsf{d}(\mathrm{F}_1,\mathrm{I}_s) + \mathsf{d}(\mathrm{I}_s,\mathrm{F}_2) + r\cos(\nu_s+\varphi)}{c}.$$

Then, the TDS at the UE is given by $\Delta\tau^{\mathrm{A}} =$

$$\max_{1\le s\le S}\tau_s^{\mathrm{A}} - \min_{1\le s\le S}\tau_s^{\mathrm{A}} = \frac{r}{c}\left(\cos(\nu_{\bar{S}}+\varphi) - \cos(\nu_{\bar{s}}+\varphi)\right), \tag{50}$$

where we used the constant sum-distance property of the ellipse stated in Theorem 3, i.e., $\mathsf{d}(\mathrm{F}_1,\mathrm{I}_s) + \mathsf{d}(\mathrm{I}_s,\mathrm{F}_2) = \lambda\ \forall s$, and the definition of $\bar{S}$, $\bar{s}$ as in the statement of the Proposition. Using the trigonometric identity of the difference between two cosines in (50), (48) follows. Finally, using the sine rule [38, Sec. 12.7] in triangle $\mathrm{F}_1\mathrm{I}_s\mathrm{F}_2$, we get $\nu_s \triangleq \sin^{-1}\left(\{\|\mathbf{q}_s\|_2/\|\mathbf{q}_s - \bar{\mathbf{p}}\|_2\}\sin(\chi_s)\right)$, where χ_s can be determined as $\chi_s = \tan^{-1}([\mathbf{q}_s]_2/[\mathbf{q}_s]_1) - \omega$ (see Fig. 5.) Collecting all these terms into (50) completes the proof. ■

From Proposition 1, we see that the TDS at an arbitrary UE scales at most linearly with the distance between the UE and the centroid within the hotspot zone. In particular, if the UE is located in a square hotspot zone with side length $2d_0$, the maximum TDS experienced at a UE is $\Delta\tau = \frac{2\sqrt{2}d_0}{c}$ and is obtained when the UE is located at a corner of the hotspot region and $\varphi + (\nu_{\bar{S}} + \nu_{\bar{s}})/2 = \nu_{\bar{s}} - \nu_{\bar{S}} = \pi/2$. The minimum TDS is 0 and is obtained when the UE is at the centroid ($r = 0$) or $\varphi + (\nu_{\bar{S}} + \nu_{\bar{s}})/2$ is an integer multiple of π. In the sequel, for a given deployment of the IRSs, we model the TDS as a random variable $\Delta\tau \overset{\text{i.i.d.}}{\sim} \mathcal{U}[0, 2\sqrt{2}d_0/c]$ across UEs. Then, similar to Theorem 2, we characterize the average sum-rate obtained under a time-division multiple access (TDMA) of UEs over the hotspot region in the following result.

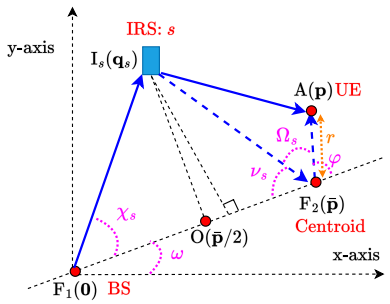

Fig. 5: Computing the TDS at an arbitrary UE.

Theorem 4. *Consider an mmWave OFDM system with K SCs where a BS serves UEs within a hotspot zone of radius d_0 using S distributed IRSs as shown in Fig. 4, each with $M = M^*$ elements as in Theorem 1. When the IRSs are placed on an ellipse whose focal points are given by the locations of BS and the centroid of the hotspot zone, the average achievable sum-rate, $\bar{R}_D^{\mathrm{opt}}$, within the hotspot region obeys*

$$\bar{R}_D^{\mathrm{opt}} \ge \mathsf{R}_{\min}^{\mathrm{opt}} \triangleq \frac{1}{K + N_{CP}^D}\sum_{k=1}^{K}\log_2\left(1 + \frac{p_k\sigma_{\mathrm{h}}^2}{\sigma^2}M^2(1-\epsilon)^2 \times \left[S^2\,\mathrm{sinc}^2\left(\frac{2\sqrt{2}d_0 f_k}{c}\right) + S\left\{1 - \mathrm{sinc}^2\left(\frac{2\sqrt{2}d_0 f_k}{c}\right)\right\}\right]\right),$$

where the parameters N_{CP}^D, p_k, σ^2, σ_{h}^2 and ϵ are the same as defined in the statement of Theorem 2.

Proof. For a hotspot zone shaped in the form of a square with semi-side length d_0, the farthest distance a UE can be located from the centroid is $\sqrt{2}d_0$. Then, using Proposition 1, the proof follows by setting $T_0 = 2\sqrt{2}d_0/c$ in Theorem 2. ■

Theorem 4 explicitly characterizes a lower bound on the achievable sum-rate as a function of the parameters of the hotspot region, unlike the characterization in Theorem 2, which is for some value of the maximum TDS, T_0, introduced by the IRSs. Also, Theorem 2 characterizes the rate at a given UE location when the IRSs are deployed such that the TDS at the UE is $\mathcal{U}[0, T_0]$. To obtain Theorem 4, we deploy the IRSs on an ellipse and consider a UE deployed in a small hotspot region such that the TDS across the UE locations is $\mathcal{U}[0, 2\sqrt{2}d_0/c]$. In particular, for smaller hotspot sizes, $\mathrm{sinc}^2(2\sqrt{2}d_0 f_k/c) \approx 1 - 8\pi^2 d_0^2 f_k^2/3c^2$. As a result, the channel gain on each SC scales as $S^2 - 8\pi^2 d_0^2 f_k^2\left(S + S^2\right)/3c^2$. Thus, for a fixed M, S, the array gain at any UE within the hotspot and not located at its centroid deviates away from the full array gain of S^2M^2 at no more than a rate of $\mathcal{O}(d_0^2)$ when the IRSs are placed on the circumference of an ellipse as shown in Fig. 4. Further, an array gain of at least SM^2 is obtained on all SCs, in line with the foregoing discussions.

V. Distributed IRSs Enable Angle Diversity

Thus far, we have discussed the advantages of a distributed design in mitigating the SW effects by parallelizing the spatial delays. Yet another useful characteristic of a distributed implementation is the diversity benefits that multiple IRSs can bring into the system [39]. In light of this, we now demonstrate

a different flavor of how distributed IRSs can aid in mitigating the SW effects. Specifically, in the following, we evaluate the ρ-outage probability on SC-k, $k=1,\ldots,K$, defined as

$$\mathbb{P}_{\rho}^{k} \triangleq \mathsf{Pr}\left(\left\{\phi_1,\ldots,\phi_S : |H[k]|^2 \le \rho\right\}\right), \tag{51}$$

where $H[k]$ is UE's channel on SC-k. Our result shows that as long as the target channel gain is below an upper bound ρ_D^k, the outage probability decreases exponentially with the number of IRSs. On the other hand, the outage probability of a centralized IRS is bounded away from zero regardless of the value of (a large) N, the number of IRS elements.

Theorem 5. *Let the IRSs be tuned to match the cascaded channel angle on the carrier frequency, i.e., at $f_k=0$. Then, on SC-k, the ρ-outage probability*

1) of an M-element S-distributed IRSs obeys

$$\mathbb{P}_{\rho}^{k} \le e^{-2S\left(\left\{1-\frac{\sqrt{\rho}}{SM\xi\sigma_{\mathrm{h}}^{min}}\right\}\frac{24f_c^2}{\pi^2M^2f_k^2}-\mu_X^{max}\right)^2}, \rho\in(0,\rho_D^k), \tag{52}$$

where $\rho_D^k \triangleq M^2S^2\xi^2(\sigma_{\mathrm{h}}^{min})^2\left(1-\mu_X^{max}\frac{\pi^2M^2f_k^2}{24f_c^2}\right)$, $\mu_X^{max} \triangleq \max\limits_{s\in[S]}\left\{\frac{1}{2}-\frac{\sin\left(2\phi_s^{(2)}\right)-\sin\left(2\phi_s^{(1)}\right)}{4\left(\phi_s^{(2)}-\phi_s^{(1)}\right)}\right\}$ and $[\phi_s^{(1)},\phi_s^{(2)}]$ denotes the cascaded angular range of the area covered by the sth IRS, $\sigma_{\mathrm{h}}^{min}\triangleq\min_s|\tilde{h}_s|$, and $\xi\in(0,1)$ is a constant.

2) of an N-element centralized IRS obeys

$$\mathbb{P}_{\rho}^{k} \ge 1-\frac{1}{\phi_0}\left\{\sin^{-1}\left(\frac{2f_c\sigma_{\mathrm{h}}}{\pi f_k\sqrt{\rho}}\right)\right\}, \text{ for } \rho \ge \frac{4f_c^2\sigma_{\mathrm{h}}^2}{\pi^2f_k^2c_0^2}, \tag{53}$$

where $[-\phi_0,\phi_0]\subseteq[-\pi/2,\pi/2]$ is the cascaded angular range of the area covered by the IRS, and $c_0=\sin(\phi_0)$.[8]

Proof. We prove the theorem in the same order as stated.

Distributed IRS: Using the expression for the channel gain in (13), the ρ-outage probability in (51) is simplified as: $\mathbb{P}_{\rho}^{k}$

$$\overset{(a)}{=} \mathsf{Pr}\left\{\left(\sum_{s=1}^{S}|\tilde{h}_s|\cos(\zeta_{s,k})\,\mathrm{sinc}\left(\frac{Mf_k}{2f_c}\sin(\phi_s)\right)\right)^2 + \left(\sum_{s=1}^{S}|\tilde{h}_s|\sin(\zeta_{s,k})\,\mathrm{sinc}\left(\frac{Mf_k}{2f_c}\sin(\phi_s)\right)\right)^2 \le \rho/M^2\right\}$$
$$\le \mathsf{Pr}\left\{\left(\sum_{s=1}^{S}|\tilde{h}_s|\cos(\zeta_{s,k})\,\mathrm{sinc}\left(\frac{Mf_k}{2f_c}\sin(\phi_s)\right)\right)^2 \le \rho/M^2\right\},$$

where in (a), $\zeta_{s,k}\triangleq\pi(M-1)f_k\sin(\phi_s)/2f_c$. By design, $\zeta_{s,k}\ll\pi/2$, so that $\cos(\zeta_{s,k})>\xi>0$, for $s\in[S]$ and some constant ξ. Using the definition of $\sigma_{\mathrm{h}}^{\min}$, we upper bound the above as

$$\mathbb{P}_{\rho}^{k} \le \mathsf{Pr}\left(\sum_{s=1}^{S}\mathrm{sinc}\left(\frac{Mf_k}{2f_c}\sin(\phi_s)\right)\le\sqrt{\rho}\Big/M\xi\sigma_{\mathrm{h}}^{\min}\right). \tag{54}$$

Now, by using the 1st order Taylor's series, $\mathrm{sinc}(x)\ge 1-\pi^2x^2/6$; so, we can further upper bound (54) as

$$\mathbb{P}_{\rho}^{k} \le \mathsf{Pr}\left(\sum_{s=1}^{S}\left\{1-\frac{\pi^2M^2f_k^2}{24f_c^2}\sin^2(\phi_s)\right\}\le\sqrt{\rho}\Big/M\xi\sigma_{\mathrm{h}}^{\min}\right)$$
$$= \mathsf{Pr}\left(\sum_{s=1}^{S}\sin^2(\phi_s)\ge\left\{S-\frac{\sqrt{\rho}}{M\xi\sigma_{\mathrm{h}}^{\min}}\right\}\frac{24f_c^2}{\pi^2M^2f_k^2}\right). \tag{55}$$

For $s=1,\ldots,S$, $\phi_s\sim\mathcal{U}[\phi_s^{(1)},\phi_s^{(2)}]$ are independent across IRSs, so that $X_s\triangleq\sin^2(\phi_s)$ are also independent random variables with mean $\mu_{X_s}\triangleq\mathbb{E}[\sin^2(\phi_s)]$ given by

$$\mu_{X_s}=\frac{1}{\phi_s^{(2)}-\phi_s^{(1)}}\int_{\phi_s^{(1)}}^{\phi_s^{(2)}}\sin^2(\phi)\mathrm{d}\phi=\frac{1}{2}-\frac{\sin\left(2\phi_s^{(2)}\right)-\sin\left(2\phi_s^{(1)}\right)}{4\left(\phi_s^{(2)}-\phi_s^{(1)}\right)}.$$

Let $\mu_X\triangleq\sum_{s=1}^{S}\mu_{X_s}$. Then, we simplify (55) as: $\mathbb{P}_{\rho}^{k}$

$$\le \mathsf{Pr}\left(\sum_{s=1}^{S}(X_s-\mu_{X_s})\ge\left\{S-\frac{\sqrt{\rho}}{M\xi\sigma_{\mathrm{h}}^{\min}}\right\}\frac{24f_c^2}{\pi^2M^2f_k^2}-\mu_X\right) \tag{56}$$
$$\overset{(b)}{\le} \mathsf{Pr}\left(\sum_{s=1}^{S}(X_s-\mu_{X_s})\ge\left\{S-\frac{\sqrt{\rho}}{M\xi\sigma_{\mathrm{h}}^{\min}}\right\}\frac{24f_c^2}{\pi^2M^2f_k^2}-S\mu_X^{\max}\right) \tag{57}$$
$$\overset{(c)}{\le} e^{-2S\left(\left\{1-\frac{\sqrt{\rho}}{SM\xi\sigma_{\mathrm{h}}^{\min}}\right\}\frac{24f_c^2}{\pi^2M^2f_k^2}-\mu_X^{\max}\right)^2},$$

where in (b), we upper bounded the probability by lower bounding the tail in (56) using $\mu_X^{\max}\triangleq\max_{s\in[S]}\mu_{X_s}$; in (c), since $\rho\in(\rho_{\mathrm{D}}^k,1)$, the tail value in (57) is positive, and we used the Hoeffding's inequality for bounded random variables [40], i.e., $0\le X_s\le 1\ \forall s\in[S]$. This completes the proof of (52).

Centralized IRS: Consider the complementary probability

$$\bar{\mathbb{P}}_{\rho}^{k} \triangleq \mathsf{Pr}\left(\left\{\phi : |H[k]|^2 \ge \rho\right\}\right). \tag{58}$$

Upon simplifying (58) similar to the above, we get

$$\bar{\mathbb{P}}_{\rho}^{k} = \mathsf{Pr}\left(\mathrm{sinc}\left(Nf_k\sin(\phi)\Big/2f_c\right)\ge\sqrt{\rho}\Big/N\sigma_{\mathrm{h}}\right) \tag{59}$$
$$\overset{(d)}{\le} \mathsf{Pr}\left(|\sin(\phi)|\le 2f_c\sigma_{\mathrm{h}}\Big/\pi f_k\sqrt{\rho}\right) \overset{(e)}{=} \frac{1}{\phi_0}\sin^{-1}\left(\frac{2f_c\sigma_{\mathrm{h}}}{\pi f_k\sqrt{\rho}}\right),$$

where in (d), we used $\mathrm{sinc}(x)\le 1/\pi|x|$, and this upper bounds the probability in (59); and in (e), for the values of ρ as in the statement of the theorem, with $\phi\sim\mathcal{U}[-\phi_0,\phi_0]$, we used the cumulative distribution function of $Y\triangleq|\sin(\phi)|$ given by

$$F_Y(\kappa)=\frac{1}{\phi_0}\int_0^{\kappa}\frac{1}{\sqrt{1-y^2}}\mathrm{d}y, \text{ if } \kappa\in(0,c_0),$$

with $\kappa = 2f_c\sigma_{\mathrm{h}}\Big/\pi f_k\sqrt{\rho}$. Computing the complementary probability completes the proof of (53) and the theorem. ∎

Thus, with high probability, while a centralized IRS severely degrades the achievable array gain under the SW effect, a distributed IRS prevents the adverse impact of the B-SP effect. The exponential fall of $\mathbb{P}_{\rho}^{k}$ in S with distributed IRSs is due to the *angle* diversity provided by multiple IRSs, i.e., each IRS provides a path at the UE whose cascaded angle is independent of other IRSs. This advantage is in addition to parallelizing the spatial delays across the IRSs.

[8] We consider a symmetrical angular range for ease of presentation. The approach easily extends to any arbitrary angular interval.

The upper bound on the target array gain, ρ_D^k, is the product of $M^2S^2\xi^2(\sigma_{\rm h}^{\min})^2$, the maximum array gain obtainable from S IRSs with M elements each, and $\left(1-(\mu_X^{\max}\pi^2M^2f_k^2/24f_c^2)\right)$, which captures the unavoidable loss in array gain due to the spatial delay spread incurred by an M-element IRS. The value of the 2nd term depends on the angular range $[\phi_s^{(1)},\phi_s^{(2)}]$ seen by the IRSs. If the interval is narrow and concentrated about 0, then this term is nearly 1. Also, as $\mu_X^{\max}$ decreases, the outage probability in (52) decreases and ρ_D^k increases, allowing for better channel gains from the system. On the other hand, in the centralized scenario, as N increases, the SW effect kicks in, and the outage probability in (53) at any f_k other than the central SC remains bounded away from zero for all $\rho=\mathcal{O}(N^2)$. Notably, as the angular range widens, the outage probability becomes high even at a moderate target SNR.

VI. Numerical Results and Discussions

We now illustrate our findings through Monte Carlo simulations. Unless mentioned otherwise, the BS is positioned at the origin $\mathbf{0}$, while the UE can be located within a rectangular hotspot region $\mathcal{R}_u$ with diagonally opposite corners specified by $[90,30]^T$ and $[110,50]^T$. The multiple IRSs are located on an ellipse with $\lambda=140$. The path loss for each link is modeled as $\mathsf{PL}=C_0(d_{\rm ref}/d)^\chi$, where $C_0=-50$ dB is the reference distance path loss measured at $d_{\rm ref}=1$ meter, d is the link distance, and χ is the path-loss exponent, set equal to 2 for both BS-IRS and IRS-UE links. We consider an OFDM system with $W=400$ MHz, $K=2000$ SCs, and $f_c=30$ GHz, assisted by an IRS with $N=1024$ elements [30], [41], [42]. Further, we consider a *transmit* SNR of $P/\sigma^2=130$ dB.

A. Results for Zero Temporal Delay Spread: $T_0=0$

1) Channel gain: For the zero TDS scenario, we consider that the UE is located at $\bar{\mathbf{p}}=\mathbb{E}_{\mathbf{p}\sim\mathrm{f}_\mathbf{p}}[\mathbf{p}]$, the centroid of the distribution of UE locations within the region $\mathcal{R}_u$. In this case, since the IRSs are positioned as per Theorem 3, the signals via the paths from all the IRSs arrive at the UE simultaneously, leading to zero TDS. In Fig. 6, we plot the channel gain (normalized by the path loss) at the UE vs. the baseband SC frequency for different values of M, the number of elements at each IRS. Each curve corresponds to the system with $S=N/M$ IRSs, where the IRSs are positioned on the ellipse such that $\phi_s=90^\circ\ \forall s$, capturing the worst-case B-SP effect. First, for $M=1024, S=1$, which denotes the centralized IRS case, the channel obtains the full array gain of N^2 only at $f_k=0$ (i.e., at f_c) and decays by several dB on SCs away from $f_k=0$, illustrating the B-SP effect. When $M<N$, i.e., $S>1$, the channel gain becomes flatter across the BW and eventually achieves the full-array gain of N^2 on all SCs, illustrating the mitigation of the B-SP effect using multiple distributed IRSs. We also validate Theorem 1 for $\epsilon\approx 0.3$, which ensures that the channel gain on all SCs is within the HPBW of the IRS beam (note the 3 dB mark.) Using (10) for $\epsilon=0.3$, we get $M=128$, and we plot the channel gain for this system and benchmark it with the theoretical gain of $(1-\epsilon)^2N^2$ as in Theorem 1. The gain is clearly above the benchmark on all SCs, in line with Theorem 1.

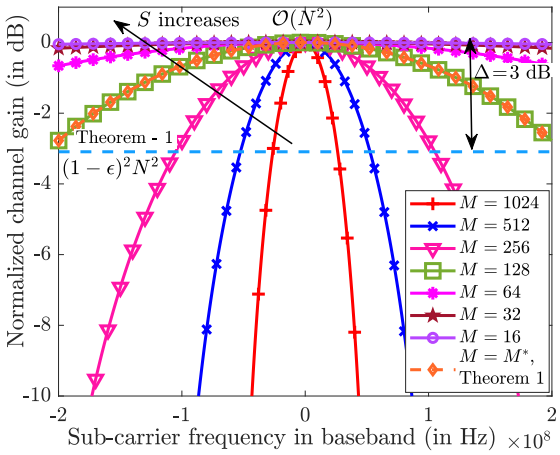

Fig. 6: Mitigating B-SP effects via distributed IRSs for $N=1024$.

2) Sum-rate: Next, in Fig. 7, we plot the achievable sum-rate vs. the transmit SNR P/σ^2 for the distributed system and contrast it with the centralized IRS setup, under uniform transmit power allocation across the SCs. We consider systems with $M=100,175,250$, which correspond to channel gains that are at least $66\%,20\%$, and 2% of the peak array gain of N^2 over the entire BW. The sum-rate of the distributed setup is better than the centralized version, and this gets more pronounced as M decreases. The reasons for this are two-fold:

1) The B-SP effect reduces in the distributed setup due to the smaller aperture delays and angle diversity effects (Sec. III-A and Sec. V.) So, the per-SC rate and the overall sum-rate increase as S (M) increases (decreases.)
2) The CP overheads are larger in the centralized case compared to the distributed case. This is due to the parallelization of aperture delays, resulting in a smaller channel delay spread in the latter. Thus, the centralized IRS suffers a further loss in the achievable sum-rate.

The plot also confirms that the scaling law derived in Theorem 2 indeed lower-bounds the achievable rate for the distributed IRS scenario. Further, we compare the performance of the distributed IRS solution against the existing approach of using TTDs as described in [18]–[24]. TTDs apply an additional delay at each IRS element and counteract the signal delay across the IRS, thereby eliminating the SW and the resulting B-SP effects. However, this comes at the cost of additional complexities: 1) the number of TTDs scales with N, requiring more hardware & space; 2) high-resolution TTDs are needed for precise delay compensation, which consumes power and 3) a sophisticated full duplex capability at the IRS to simultaneously receive, delay and reflect signals toward the UE, all of which defeat the energy-efficient nature of IRSs. From Fig. 7, the distributed IRS achieves the same performance obtained using TTDs without any extra complexity. Finally, we demonstrate that our approach achieves better performance than an $N/4\times 4$ uniform planar array (UPA) in place of the ULA. Although a UPA-based IRS outperforms its ULA counterpart with the same N owing to the reduced impact of the B-SP effect in the former [27], it does not fully eliminate the B-SP effect. In contrast, our approach is IRS geometry-agnostic and effectively mitigates the B-SP effect to

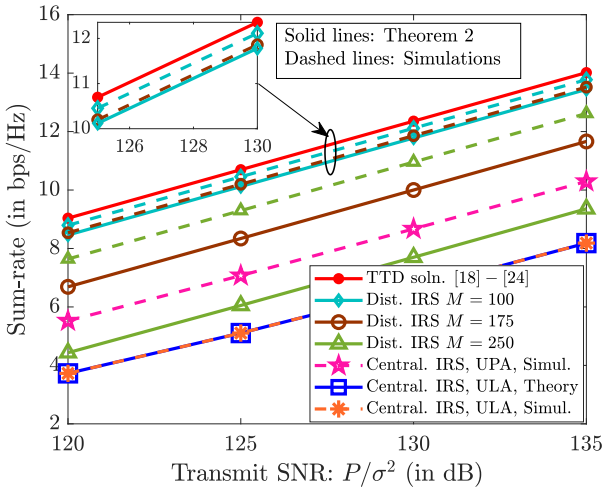

Fig. 7: Sum-rate vs. Transmit SNR.

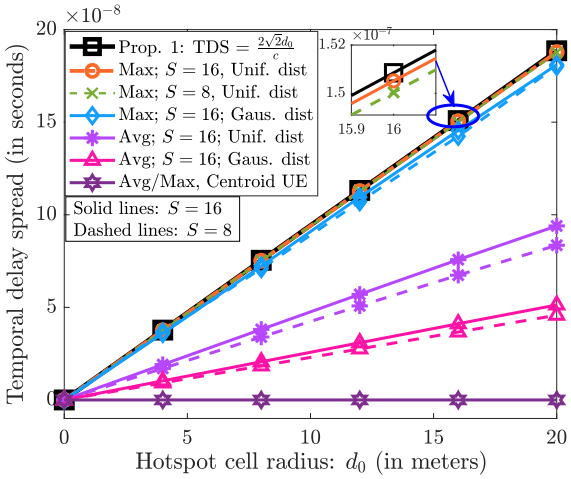

Fig. 8: TDS vs. d_0 for different number of IRSs, S.

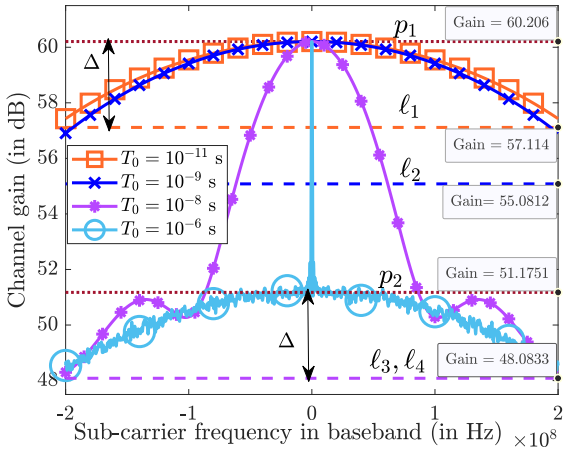

Fig. 9: Mitigating B-SP effects with finite TDS for $\Delta = 3$ dB.

deliver superior performance.

B. Results for Non-zero Temporal Delay Spread: $T_0 > 0$

We now analyze how distributed IRSs can alleviate the B-SP effect even when the IRSs introduce non-zero TDS in the channel at the UE placed at an arbitrary location within the hotspot zone $\mathcal{R}_u$ of radius d_0, as illustrated in Fig. 4.

1) Amount of TDS: We first assess the amount of TDS experienced by a UE located away from the centroid. In Fig. 8, we plot TDS versus d_0 for different S, the number of IRSs, considering two distributions for the UE locations: 1) a uniform distribution within $\mathcal{R}_u$, and 2) a 2-dimensional truncated Gaussian distribution with mean $\bar{\mathbf{p}}$ and standard deviation $\sigma_U = d_0/3$, with its support being $\mathcal{S}_U \triangleq \{\mathbf{p} \in \mathbb{R}^2 : \|\mathbf{p} - \bar{\mathbf{p}}\|_\infty \leq d_0\}$. We observe that both the average TDS and the maximum TDS increase as d_0 increases. This is because the IRS placements are optimized to achieve zero TDS only at the centroid of the location distribution within $\mathcal{R}_u$, and the TDS increases as we move away from the centroid (see Proposition 1). Furthermore, since the truncated Gaussian distribution is more concentrated around the centroid than the uniform distribution, the TDS in the former is smaller than that in the latter, but both are well upper-bounded by the maximum TDS predicted by Proposition 1.

2) Channel gain: In Fig. 9, considering the worst-case B-SP effect, we plot the channel gain vs. the SC frequency for different values of T_0. The sampling time is $T_s = 1/W = 2.5 \times 10^{-9}$ seconds. We also plot the following equations:

$$p_1 : g_1(f_k) = N^2; f_k \in [-W/2, W/2].$$
$$\ell_1 : g_2(f_k) = (1-\epsilon)^2 M^2 \left[S^2 h^2(10^{-11}) + S\left(1 - h^2(10^{-11})\right)\right]$$
$$\ell_2 : g_3(f_k) = (1-\epsilon)^2 M^2 \left[S^2 h^2(10^{-9}) + S\left(1 - h^2(10^{-9})\right)\right]$$
$$p_2 : g_4(f_k) = SM^2; f_k \in [-W/2, W/2].$$
$$\ell_3 : g_5(f_k) = (1-\epsilon)^2 M^2 \left[S^2 h^2(10^{-8}) + S\left(1 - h^2(10^{-8})\right)\right]$$
$$\ell_4 : g_6(f_k) = (1-\epsilon)^2 M^2 \left[S^2 h^2(10^{-6}) + S\left(1 - h^2(10^{-6})\right)\right]$$

where $h^2(t) \triangleq \text{sinc}^2(Wt/2)$. The lines $\ell_1, \ell_2, \ell_3, \ell_4$ represent the minimum channel gains in non-zero TDS scenarios, unlike the zero gains that occur from the B-SP effect. As long as $T_0 < T_s$ (i.e., when the paths from all IRSs arrive within the same sampling interval), the IRS phase configurations can compensate for differential delays across the IRSs, and provide a full array gain of $S^2M^2 = N^2$ on all SCs, with only a minor loss due to the permissible B-SQ (here, it is 3 dB.) However, when $T_0 \geq T_s$ and as T_0 increases, the array gain over the SCs decreases and flattens below N^2, as described in Theorem 4. For large T_0 (e.g., 10^{-5} s), the channel gain flattens at around approximately $\mathcal{O}(SM^2)$, with a 3 dB residual B-SQ loss. This is because, in this case, the gain at the UE is obtained only via the incoherent superposition of signals from the IRSs. However, at the SC where $f_k = 0$, since the IRSs' phase shifts can fully compensate for any differential path delay, the channel gain still scales as N^2. Thus, the distributed IRS effectively mitigates the B-SP effect and ensures a flat response across the BW, even after accounting for the nonzero TDS.

3) Average sum-rate: In Fig. 10, we evaluate the average sum-rate of the distributed IRS system, designed for $\epsilon \approx 0.3$, by plotting it against the transmit SNR, P/σ^2, for $N = 1024$ and 4096. The results are averaged over multiple UE locations within a hotspot defined by $\bar{\mathbf{p}} = [80, 80]^T$, $d_0 = 12$ meters, and the IRSs placed on an ellipse with $\lambda = 160$. For $N = 1024$, the distributed IRS significantly outperforms the centralized IRS, even after accounting for the nonzero TDS in the former setup. Further, the curve obtained based

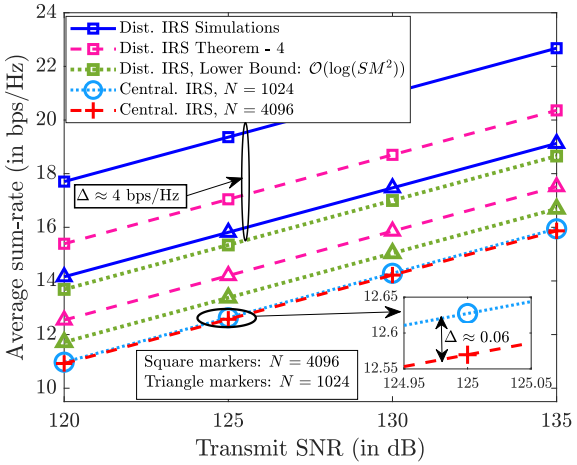

Fig. 10: Sum-rate vs. Transmit SNR with non-zero TDS.

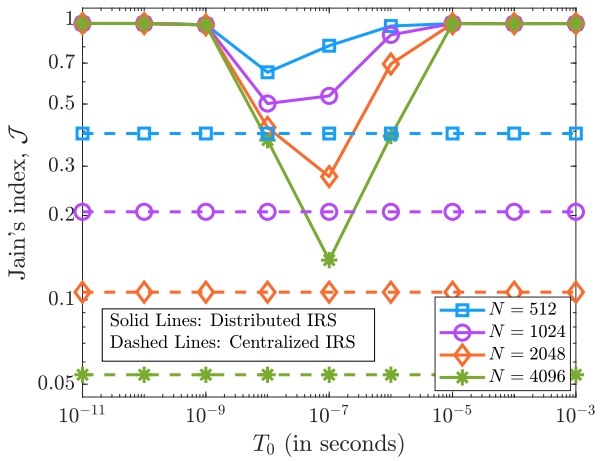

Fig. 11: Jain's index, $\mathcal{J}$ across SCs for $K = 2000$.

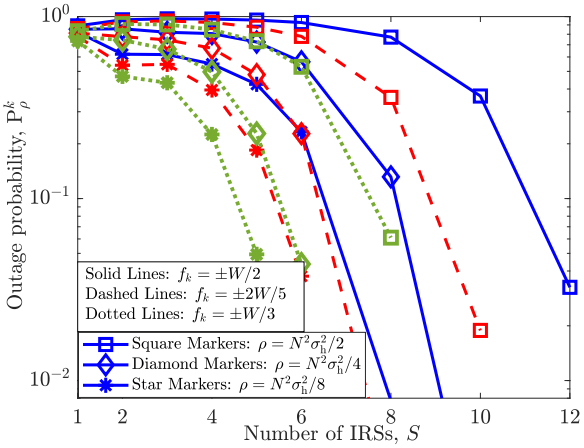

Fig. 12: B-SP induced outage probability versus S.

on Theorem 4 (labeled `Dist. IRS Theorem 4`) lower-bounds the empirical sum-rate, confirming the accuracy of our analysis. Additionally, we show the worst-case lower bound on the rate that scales as $\mathcal{O}(\log(SM^2))$ on the plot. The gap between the achievable sum-rate and this lower bound is high, showing that our solution can, in fact, perform much better than the incoherent gain of $\mathcal{O}(\log(SM^2))$ on all SCs. Finally, when the number of IRS elements quadruples from $N = 1024$ to $N = 4096$, the rate improves by 4 bps/Hz, demonstrating that our method achieves the full array gain of $\mathcal{O}(N^2)$ (since $\log_2((4N)^2) = 4 + \log_2(N^2)$). In contrast, the sum-rate using a centralized IRS marginally reduces due to the B-SP effect.

4) Jain's index: Next, in Figure 11, we demonstrate the flatness in the channel gain across SCs by plotting the Jain's index as a function of T_0. The Jain's index is calculated using the channel gains on different SCs as

$$\mathcal{J} \triangleq \frac{\left(\sum_{k=1}^{K}|H[k]|^2\right)^2}{K\sum_{k=1}^{K}|H[k]|^4}.$$

It is known that $\frac{1}{K} \leq \mathcal{J} \leq 1$, with $\mathcal{J} = 1$ achieved when the channel gains are equal on all SCs. In Fig. 11, we depict Jain's index for both the centralized and distributed IRS setups for different values of N. For any given N, the index $\mathcal{J}$ for a distributed IRS is approximately 1 for small T_0, then decreases below 1 for moderate T_0, and returns to 1 for large T_0. This behavior can be explained as follows. For small T_0, the channel gain uniformly scales as $\mathcal{O}(N^2)$ on all SCs within the HPBW of the main lobe, yielding $\mathcal{J} \approx 1$. As T_0 increases, the channel gain fluctuates between $\mathcal{O}(SM^2)$ and $\mathcal{O}(S^2M^2)$ across different SCs as illustrated in Fig. 9, causing $\mathcal{J}$ to drop below 1. When T_0 becomes high, $\mathcal{J}$ increases again to 1 because the channel exhibits an almost flat response within 3 dB of the peak gain of $\mathcal{O}(SM^2)$ due to the incoherent addition of signals from the IRSs. Since S increases with N (M remains constant since we design the system for $\epsilon \approx 0.3$), the gap between SM^2 and S^2M^2 increases as N increases, leading to larger fluctuations in the channel gain at moderate T_0. This results in a lower Jain's index $\mathcal{J}$ for intermediate T_0 as N is increased. Importantly, the Jain's index obtained using a distributed IRS is much higher than in the corresponding centralized IRS scenario, showing that the distributed IRS can effectively flatten the channel frequency response even after accounting for the nonzero TDS.

C. Diversity Benefits of Distributed IRSs

We next showcase how distributed IRSs can also leverage diversity benefits to further mitigate the B-SP effects in Fig. 12. To this end, we simulate the B-SP induced outage probability $\mathbb{P}_\rho^k$ as a function of S for various UE location realizations. The plot clearly shows that $\mathbb{P}_\rho^k$ decreases exponentially with the number of IRSs, in line with Theorem 5. Multiple IRSs provide independent paths with different channel angles, and the resulting angle diversity makes it unlikely that all IRSs experience the worst-case spatial delay spread. Further, $\mathbb{P}_\rho^k$ decreases as ρ decreases, in line with the inferences from Theorem 5. Note that $\rho = N^2\sigma_h^2/2^\ell$ corresponds to an allowed loss of 3ℓ dB relative to the peak array gain of N^2. Thus, larger degradation in the array gain due to the B-SP is less likely to happen with distributed IRSs. Similarly, since the B-SP effects are less pronounced near the center SC, $\mathbb{P}_\rho^k$ reduces as $|f_k|$ is near 0, in line with Theorem 5. Thus, distributed IRSs also provide instantaneous benefits to minimize the SW and the resulting B-SP effects.

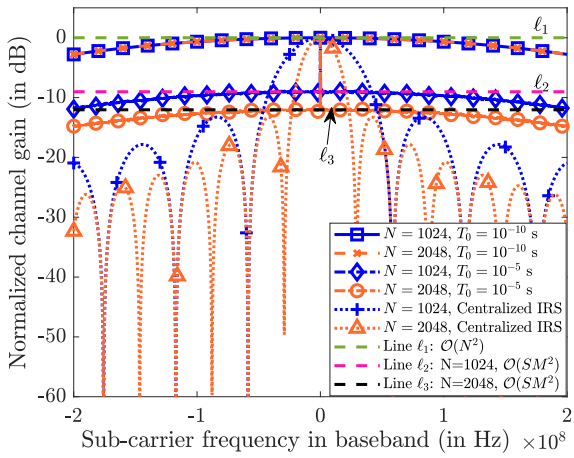

Fig. 13: Channel gains in centralized vs. distributed IRSs.

D. Array Gain Using Distributed vs. Centralized IRS

Finally, in Fig. 13, we summarize a big picture of the solution by comparing the channel gain obtained using a distributed IRS with the conventional centralized IRS. We observe that distributed IRSs can completely combat the B-SP effect and provide a significantly better array gain on all SCs. Although the channel gain with distributed IRSs concentrates about $\mathcal{O}(SM^2)$ when the TDS is arbitrarily large and is less than $\mathcal{O}(N^2)$, this still avoids deep nulls, ensuring that the IRS can focus on the desired UE on all SCs. In fact, even the reduced gain with distributed IRSs due to large TDS is much better than the array gain using a centralized IRS over all SCs other than the center SC. Thus, the distributed IRSs effectively mitigate the SW effect (and hence the B-SP) and outperform the centralized IRS at almost no additional complexity.

VII. Conclusions

We tackled the issue of SW and the resulting B-SP effects in IRS-aided wideband systems by identifying that the SW effect primarily stems from the linear increase of spatial delay spread across the IRS aperture. In this view, we proposed a distributed IRS design that a) parallelizes spatial delay and b) utilizes angle diversity, which collectively mitigates the SW and B-SP effects. In particular, we detailed how to determine the number of elements at each IRS, the number of IRSs, and the placement of the IRSs that can eliminate the SW effects while procuring the optimal array gain over the entire BW for a given total number of IRS elements. Our solution provides uniformly positive benefits over the full BW at any UE with no significant complexity compared to existing methods. Potential future work can include extending the solutions to account for near-field effects and UE mobility scenarios.

References

[1] L. Yashvanth, C. R. Murthy, and B. D. Rao, "Distributed IRSs mitigate spatial wideband & beam split effects," in *Proc. IEEE Int. Conf. Acoust. Speech Signal Process. (ICASSP)*, Apr. 2025, pp. 1–5.

[2] E. Basar, M. Di Renzo, J. De Rosny, M. Debbah, M.-S. Alouini, and R. Zhang, "Wireless communications through reconfigurable intelligent surfaces," *IEEE Access*, vol. 7, pp. 116 753–116 773, 2019.

[3] Q. Wu and R. Zhang, "Towards smart and reconfigurable environment: Intelligent reflecting surface aided wireless network," *IEEE Commun. Mag.*, vol. 58, no. 1, pp. 106–112, 2020.

[4] E. Björnson *et al.*, "Reconfigurable intelligent surfaces: A signal processing perspective with wireless applications," *IEEE Signal Process. Mag.*, vol. 39, no. 2, pp. 135–158, Mar. 2022.

[5] Z. Zhang, L. Dai, X. Chen, C. Liu, F. Yang, R. Schober, and H. V. Poor, "Active RIS vs. passive RIS: Which will prevail in 6G?" *IEEE Trans. Commun.*, vol. 71, no. 3, pp. 1707–1725, Mar. 2023.

[6] B. Wang, F. Gao, S. Jin, H. Lin, and G. Y. Li, "Spatial- and frequency-wideband effects in millimeter-wave massive MIMO systems," *IEEE Trans. Signal Process.*, vol. 66, no. 13, pp. 3393–3406, Jul. 2018.

[7] S. Ma, W. Shen, J. An, and L. Hanzo, "Wideband channel estimation for IRS-aided systems in the face of beam squint," *IEEE Trans. Wireless Commun.*, vol. 20, no. 10, pp. 6240–6253, Oct. 2021.

[8] A. Abdallah *et al.*, "Deep-learning based channel estimation for RIS-aided mmwave systems with beam squint," in *Proc. IEEE Int. Conf. Commun.*, May 2022, pp. 1269–1275.

[9] Y. Chen, J. Tan, M. Hao, R. MacKenzie, and L. Dai, "Accurate beam training for RIS-assisted wideband terahertz communication," *IEEE Trans. Commun.*, vol. 71, no. 12, pp. 7425–7440, Dec. 2023.

[10] K. Keykhosravi *et al.*, "RIS-enabled SISO localization under user mobility and spatial-wideband effects," *IEEE J. Sel. Topics Signal Process.*, vol. 16, no. 5, pp. 1125–1140, Aug. 2022.

[11] Y. Chen, D. Chen, and T. Jiang, "Beam-squint mitigating in reconfigurable intelligent surface aided wideband mmwave communications," in *Proc. IEEE Wireless Commun. Netw. Conf.*, Mar. 2021, pp. 1–6.

[12] Y. Jiang *et al.*, "Beamforming design for RIS-aided THz wideband communication systems," in *Proc. IEEE 24th Int. Workshop Signal Process. Adv. Wireless Commun. (SPAWC)*, Sep. 2023, pp. 296–300.

[13] J. Wu and B. Shim, "Frequency-dependent beamforming for RIS-assisted wideband terahertz systems," in *2023 IEEE 97th Vehicular Technology Conference (VTC2023-Spring)*, Jun. 2023, pp. 1–6.

[14] R. Li *et al.*, "Ergodic achievable rate maximization of RIS-assisted millimeter-wave MIMO-OFDM communication systems," *IEEE Trans. Wireless Commun.*, vol. 22, no. 3, pp. 2171–2184, Mar. 2023.

[15] H. Ozen and G. M. Guvensen, "A robust quantized beam-squint and interference aware statistical beamforming for RIS-aided massive MIMO," in *Proc. IEEE Int. Conf. Commun.*, May 2023, pp. 1307–1312.

[16] X. Lin *et al.*, "Beamforming on reconfigurable intelligent surface: A codebook design for spatial coverage with beam squint effect," in *Proc. IEEE Int. Conf. Commun. Workshops*, May 2023, pp. 1130–1135.

[17] Y. Kawamoto *et al.*, "Simultaneous multiple connections and increased frequency efficiency using beam squint approach for IRS-based communication," *IEEE Trans. Vehicular Technol.*, vol. 73, no. 11, pp. 17 073–17 082, Nov. 2024.

[18] H. Sun, S. Zhang, J. Ma, and O. A. Dobre, "Time-delay unit based beam squint mitigation for RIS-aided communications," *IEEE Commun. Lett.*, vol. 26, no. 9, pp. 2220–2224, Sep. 2022.

[19] R. Su *et al.*, "Wideband precoding for RIS-aided THz communications," *IEEE Trans. Commun.*, vol. 71, no. 6, pp. 3592–3604, Jun. 2023.

[20] W. Hao *et al.*, "The far-/near-field beam squint and solutions for THz intelligent reflecting surface communications," *IEEE Trans. Vehicular Technol.*, vol. 72, no. 8, pp. 10 107–10 118, Aug. 2023.

[21] F. Zhao *et al.*, "Joint beamforming optimization for IRS-aided THz communication with time delays," *IEEE Wireless Commun. Lett.*, vol. 13, no. 1, pp. 49–53, Jan. 2024.

[22] X. Su *et al.*, "Joint precoding for RIS-assisted wideband THz cell-free massive MIMO systems," *arXiv preprint arXiv:2405.07830*, 2024.

[23] J. Li *et al.*, "Holographic RIS-aided wideband communication with beam-squint mitigation," *IEEE Trans. Commun.*, pp. 1–1, 2024.

[24] ——, "User sensing in RIS-aided wideband mmwave system with beam-squint and beam-split," *IEEE Trans. Commun.*, vol. 73, no. 2, pp. 1304–1319, Feb. 2025.

[25] Z. Zhang, L. Dai, X. Chen, C. Liu, F. Yang, R. Schober, and H. V. Poor, "Active RIS vs. passive RIS: Which will prevail in 6G?" *IEEE Trans. Commun.*, vol. 71, no. 3, pp. 1707–1725, Mar. 2023.

[26] F. Gao, B. Wang, C. Xing, J. An, and G. Y. Li, "Wideband beamforming for hybrid massive MIMO terahertz communications," *IEEE J. Sel. Areas Commun.*, vol. 39, no. 6, pp. 1725–1740, Jun. 2021.

[27] W. Yan *et al.*, "Beamforming analysis and design for wideband THz reconfigurable intelligent surface communications," *IEEE J. Sel. Areas Commun.*, vol. 41, no. 8, pp. 2306–2320, Aug. 2023.

[28] G. Sun *et al.*, "Beamforming design for the distributed RISs-aided THz communications with double-layer true time delays," *IEEE Trans. Vehicular Technol.*, vol. 73, no. 3, pp. 3886–3900, Mar. 2024.

[29] J. Chen *et al.*, "Channel estimation for reconfigurable intelligent surface aided multi-user mmwave MIMO systems," *IEEE Trans. Wireless Commun.*, vol. 22, no. 10, pp. 6853–6869, Oct. 2023.

[30] L. Yashvanth and C. R. Murthy, "On the impact of an IRS on the out-of-band performance in sub-6 GHz and mmwave frequencies," *IEEE Trans. Commun.*, vol. 72, no. 12, pp. 7417–7434, Dec. 2024.
[31] H. L. Van Trees, *Optimum array processing: Part IV of detection, estimation, and modulation theory*. John Wiley & Sons, 2002.
[32] R. A. Horn and C. R. Johnson, *Matrix analysis*. Cambridge university press, 2012.
[33] H. Han *et al.*, "On half-power beamwidth of intelligent reflecting surface," *IEEE Commun. Lett.*, vol. 25, no. 4, pp. 1333–1337, Apr. 2021.
[34] F. J. Martín-Vega, J. C. Ruiz-Sicilia, M. C. Aguayo, and G. Gómez, "Emerging tools for link adaptation on 5G NR and beyond: Challenges and opportunities," *IEEE Access*, vol. 9, pp. 126 976–126 987, 2021.
[35] L. Yashvanth and C. R. Murthy, "Cascaded channel estimation for distributed IRS aided mmwave massive MIMO systems," in *Proc. IEEE Glob. Commun. Conf.*, Dec. 2022, pp. 717–723.
[36] K. Yoshikawa *et al.*, "User and passive beam scheduling scheme for liquid crystal IRS-assisted mmwave communications," in *Proc. European Conf. on Antennas and Propagation (EuCAP)*, Mar. 2024, pp. 1–5.
[37] D. Hilbert and S. Cohn-Vossen, *Geometry and the Imagination*. American Mathematical Soc., 2021, vol. 87.
[38] J. Bird, *Engineering Mathematics*. CRC Press, 2017. [Online]. Available: https://books.google.co.in/books?id=bAcqDwAAQBAJ
[39] L. Yashvanth and C. R. Murthy, "Distributed IRSs always benefit every mobile operator," *IEEE Wireless Commun. Lett.*, vol. 13, no. 11, pp. 2975–2979, Nov. 2024.
[40] M. J. Wainwright, *High-dimensional statistics: A non-asymptotic viewpoint*. Cambridge university press, 2019, vol. 48.
[41] Z. Xing *et al.*, "Location information assisted beamforming design for reconfigurable intelligent surface aided communication systems," *IEEE Trans. Wireless Commun.*, vol. 22, no. 11, pp. 7676–7695, Nov. 2023.
[42] C. You, B. Zheng, and R. Zhang, "Fast beam training for IRS-assisted multiuser communications," *IEEE Wireless Commun. Lett.*, vol. 9, no. 11, pp. 1845–1849, Nov. 2020.

L. Yashvanth (Student Member, IEEE) obtained his B. Tech (Honors) degree in Electronics and Communication Engineering from National Institute of Technology, Trichy, India, with a Gold medal in 2020. He is currently pursuing his Ph. D. in the Department of Electrical Communication Engineering, Indian Institute of Science, Bangalore, India, with a focus on intelligent reflecting surfaces for next-generation wireless communications.

He is also a recipient of the Qualcomm Innovation Fellowships and the Prime Minister's Research Fellowship, Govt. of India. His broad research interests lie in statistical signal processing and optimization of wireless communication systems.

Chandra R. Murthy (Fellow, IEEE) received the B. Tech. degree in Electrical Engineering from the Indian Institute of Technology Madras, India, in 1998, the M. S. and Ph. D. degrees in Electrical and Computer Engineering from Purdue University and the University of California, San Diego, USA, in 2000 and 2006, respectively. In Sept. 2007, he joined the Department of Electrical Communication Engineering at the Indian Institute of Science, Bangalore, India, where he is currently working as a Professor.

From 2000 to 2002, he was with Qualcomm Inc., on WCDMA baseband transceiver design and 802.11b baseband receivers. From 2006 to 2007, he was a Staff Engineer with Beceem Communications Inc., on advanced receiver architectures for the 802.16e mobile WiMAX standard. His research interests are in the areas of sparse signal recovery, energy harvesting-based communication, performance analysis, and optimization of 5G and beyond communications. Papers co-authored by him have received Student/Best Paper Awards at the NCC 2014, IEEE ICASSP 2018, IEEE ISIT 2021, IEEE SPAWC 2022, and NCC 2023. He has served on the editorial board of the IEEE SIGNAL PROCESSING LETTERS, IEEE TRANSACTIONS ON SIGNAL PROCESSING, SADHANA Journal, and the IEEE TRANSACTIONS ON COMMUNICATIONS. Currently, he is an elected member of the IEEE SAM Technical Committee and a Senior Area Editor of the IEEE TRANSACTIONS ON INFORMATION THEORY. He is a fellow of the IEEE and INAE.

Bhaskar D. Rao (Life Fellow, IEEE) received the B.Tech. degree in electronics and electrical communication engineering from the Indian Institute of Technology, Kharagpur, India, in 1979, and the M.S. and Ph.D. degrees from the University of Southern California, Los Angeles, in 1981 and 1983, respectively. Since 1983, he has been teaching and conducting research at the University of California, San Diego, La Jolla, where he is currently a Professor Emeritus and Distinguished Professor of the Graduate Division in the Electrical and Computer Engineering department. He has also been the holder of the Ericsson Endowed Chair in Wireless Access Networks and Distinguished Professor and the Director of the Center for Wireless Communications from 2008 to 2011. His research interests are in the areas of statistical signal processing, estimation theory, optimization theory, and machine learning, with applications to digital communications, speech signal processing, and biomedical signal processing. He is a pioneer in the theory and use of sparsity in signal processing applications.

His work has received several paper awards, including the 2012 Signal Processing Society (SPS) Best Paper Award for the paper "An Empirical Bayesian Strategy for Solving the Simultaneous Sparse Approximation Problem," and the Stephen O. Rice Prize Paper Award in the field of communication systems for the paper "Network Duality for Multiuser MIMO Beamforming Networks and Applications." He was elected as a fellow of IEEE in 2000 for his contributions to the statistical analysis of subspace algorithms for harmonic retrieval. He received the IEEE Signal Processing Society Technical Achievement Award in 2016 and was the recipient of the 2023 IEEE SPS Norbert Wiener Society Award. He has been a member of the Statistical Signal and Array Processing Technical Committee, the Signal Processing Theory and Methods Technical Committee, the Communications Technical Committee of the IEEE Signal Processing Society, SPS Fellow Evaluation Committee, from 2023 to 2024, and was the Chair of the Machine Learning for Signal Processing Technical Committee, from 2019 to 2020.